symmetry

MDPI

Article

Topological and Thermodynamic Entropy Measures for COVID-19 Pandemic through Graph Theory

G. Kirithiga Nandini [1], R. Sundara Rajan [2], A. Arul Shantrinal [2], T. M. Rajalaxmi [3], Indra Rajasingh [4] and Krishnan Balasubramanian [5,*]

1 Department of Computer Science and Engineering, Hindustan Institute of Technology and Science, Chennai 603 103, India; gknandini93@gmail.com
2 Department of Mathematics, Hindustan Institute of Technology and Science, Chennai 603 103, India; vprsundar@gmail.com (R.S.R.); shandrinashan@gmail.com (A.A.S.)
3 Department of Mathematics, Sri Sivasubramaniya Nadar College of Engineering, Chennai 603 110, India; laxmi.raji18@gmail.com
4 School of Advanced Sciences, Vellore Institute of Technology, Chennai 600 127, India; indrarajasingh@yahoo.com
5 School of Molecular Sciences, Arizona State University, Tempe, AZ 85287-1604, USA
* Correspondence: baluk@asu.edu

Received: 14 October 2020; Accepted: 30 November 2020; Published: 2 December 2020

Abstract: Severe acute respiratory syndrome coronavirus 2 (SARS-CoV-2) has caused the global pandemic, coronavirus disease-2019 (COVID-19) which has resulted in 60.4 million infections and 1.42 million deaths worldwide. Mathematical models as an integral part of artificial intelligence are designed for contact tracing, genetic network analysis for uncovering the biological evolution of the virus, understanding the underlying mechanisms of the observed disease dynamics, evaluating mitigation strategies, and predicting the COVID-19 pandemic dynamics. This paper describes mathematical techniques to exploit and understand the progression of the pandemic through a topological characterization of underlying graphs. We have obtained several topological indices for various graphs of biological interest such as pandemic trees, Cayley trees, Christmas trees, and the corona product of Christmas trees and paths. We have also obtained an analytical expression for the thermodynamic entropies of pandemic trees as a function of R^0, the reproduction number, and the level of spread, using the nested wreath product groups. Our plots of entropy and logarithms of topological indices of pandemic trees accentuate the underlying severity of COVID-19 over the 1918 Spanish flu pandemic.

Keywords: COVID-19; pandemic trees; Cayley trees; entropy of pandemic trees; corona product of graphs; topological indices

1. Introduction

Severe acute respiratory syndrome coronavirus 2 (SARS-CoV-2), commonly called the novel coronavirus (COVID-19), has resulted in 1.42 million deaths worldwide up to now [1,2]. The first case was detected in the city of Wuhan, China on 31 December 2019, and it was reported by Zhou et al. [3] as a pneumonia outbreak associated with a new coronavirus of bat origin. It is presently understood that the disease spreads by human-to-human or aerosol transmission via either droplet in the air or through direct or indirect contacts. An underestimated mean incubation period of 2.24–3.58 days [4] has now been revised to a median R^0 value close to 5.7 in some regions of a susceptible population. This dramatically contrasts with the previous Spanish flu virus which has a R^0 value close to 1.8. There are seven types of coronaviruses that infect humans [5], including the newly discovered SARS-CoV-2 virus. The level and duration of infectious virus replication are important factors in the

risk assessments [6]. A study on interspecies transmission of the virus and its genetic diversity can provide mitigation strategies against the infection [7].

Biological models can simulate the dynamics of the spread and genetic evolution of a disease as to how cells interact in a single patient and how genetic mutations spread across people living in different geographical locations [2,8]. Forster et al. [9] recently considered phylogenetic networks as powerful tools for understanding the genetic evolution of the coronavirus 2019. Graph models also enhance our understanding of the effect of introducing an affected individual in a pool of unaffected individuals. Recursive trees constructed from phylogenetics have provided graphical representation of microbiomes and have been proven to be powerful in the perturbations induced to genomes and proteomes by environment or toxins [10–13], and hence, graph techniques are especially suited to understand the dynamics of the COVID-19 epidemic. Furthermore, it has been shown that tree pruning methods and other efficient topological techniques can be applied to characterize various biological trees such as phylogenetic trees, epidemic trees, Cayley trees, and the lattices through graph theoretical entities [14–17]. The combinatorial theory of genetic mutations and the applications of graph theory to the computation of evolutionary genomics have been pioneered by Sellers and others [12,13,18–20]. Yun et al. [21] demonstrated the graph mining approaches in identifying the patterns in complex and large data sets such as the chemical and genome data sets.

Network models help to capture the transmission, forecast the future of the pandemic, and estimate the sequel of ongoing interventions [22]. A pandemic tree provides a pictorial representation of the epidemic dynamics where each node is connected to k other nodes, where k is an integer rounded from the R^0 value, an epidemiological measure of the degree of infection, suggesting that an infected individual in turn infects R^0 others in a susceptible population pool. Consequently, quantitative measures of a pandemic network can provide significant new insights into the epidemic dynamics. Topological indices have been developed that aid in the prediction of chemical, physical, pharmaceutical, and biological properties [23–29]. The eccentric connectivity index is one such topological index that is currently being used for modeling biological activities of chemical compounds. In anticonvulsant, anti-inflammatory, and diuretic activities, this index exhibits high degree of predictability [30]. Ghorbani et al. [31] obtained various eccentricity–entropy-based topological measures of fullerenes.

We consider several trees of biological and phylogenetic interests and corona products of graphs in order to obtain the topological measures of the associated networks. In particular, we consider several classes of recursive networks of biological importance, namely pandemic trees, Cayley trees, Christmas trees, and the corona products of Christmas trees and paths. In Section 2, basic definitions are stated, while Section 3 computes the eccentricity-based topological indices. Section 4 highlights various applications of topological indices to the COVID-19 pandemic, while in Section 5, we study the thermodynamic entropy of pandemic trees. Section 6 discusses stochasticity in pandemic tree generation. The conclusion is given in Section 7.

2. Basic Concepts

Let $G = (V(G), E(G))$ be a graph with $V(G)$ as the set of vertices and $E(G)$ as the set of edges. A tree is a connected, acyclic graph. In a binary tree, each node can have at most two descendants. It is said to be a complete binary tree if each internal node has exactly two descendants.

The length of the shortest path between two vertices x and y in a graph G is the topological distance between x and y and it is denoted by $d(x,y)$. The eccentricity value of a vertex $u \in V(G)$ denoted by $ec(u)$ is the longest distance between the vertex u and any other vertex v of G. The neighborhood of a vertex u, denoted by $n(u)$, is the set of all vertices which are adjacent to u. Let $d(u)$ denote the degree of a vertex u. For an edge $uv \in E(G)$, let $n_u(e)$ be the number of vertices lying closer to the vertex u than the vertex v and let $n_v(e)$ denote the number of vertices lying closer to the vertex v than the vertex u.

The fourth geometric-arithmetic eccentricity index was introduced by Ghorbani and Khaki [32]: as

$$GA_4(G) = \sum_{uv \in E(G)} \frac{2\sqrt{ec(u)ec(v)}}{ec(u) + ec(v)}.$$

Furthermore, the fourth Zagreb index, the fourth multiplicative Zagreb index, the sixth Zagreb index, and the sixth multiplicative Zagreb index [33,34] are defined as follows:

$$Zg_4(G) = \sum_{uv \in E(G)} (ec(u) + ec(v));$$

$$\Pi_4^*(G) = \prod_{uv \in E(G)} (ec(u) + ec(v));$$

$$Zg_6(G) = \sum_{uv \in E(G)} ec(u)\, ec(v);$$

$$\Pi_6^*(G) = \prod_{uv \in E(G)} ec(u)\, ec(v).$$

The fourth Zagreb polynomial $Zg_4(G, x)$ and the sixth Zagreb polynomial $Zg_6(G, x)$ [33,34] are defined by:

$$Zg_4(G, x) = \sum_{uv \in E(G)} x^{ec(u) + ec(v)};$$

$$Zg_6(G, x) = \sum_{uv \in E(G)} x^{ec(u)\, ec(v)}.$$

The fifth multiplicative atom bond connectivity index [33] is defined as:

$$ABC_5\Pi(G) = \prod_{uv \in E(G)} \sqrt{\frac{ec(u) + ec(v) - 2}{ec(u)\, ec(v)}}.$$

The first Zagreb index $M_1(G)$ [35] is defined as:

$$M_1(G) = \sum_{v_i \in V(G)} d_i^2.$$

The second Zagreb index $M_2(G)$ [35] of graph G is defined as:

$$M_2(G) = \sum_{v_i v_j \in E(G)} d_i d_j.$$

The Atom-bond Connectivity index (ABC) [36] is defined as:

$$ABC(G) = \sum_{v_i v_j \in E(G)} \sqrt{\frac{d_i + d_j - 2}{d_i d_j}}.$$

The Padmakar–Ivan (PI) index [37] is defined as:

$$PI(G) = \sum_{e = uv \in E(G)} [n_u(e) + n_v(e)].$$

The Szeged Index [38] is defined as:

$$Sz(G) = \sum_{e=uv \in E(G)} [n_u(e) \times n_v(e)].$$

3. Main Results for the Topological Indices

In epidemiology, R^0, the reproduction number measures the severity of the pandemic, and it is defined as the number of individuals an infected person can in turn infect in a group of susceptible population set. For example, Figure 1 shows a pandemic tree for an epidemic with an R^0 value of 4. In this section, we have obtained the eccentricity-related indices for the pandemic tree network (also called a complete k-ary tree network), Cayley tree network, Christmas trees, and the corona product of Christmas tree and a path, all of which are defined in the respective sections.

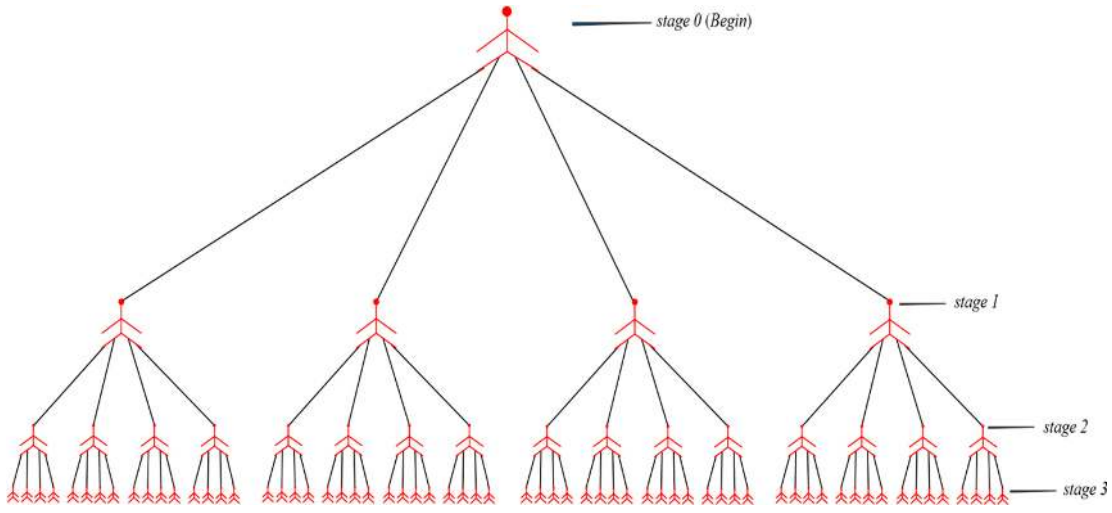

Figure 1. A pandemic tree with an epidemiological R^0 value of 4.

3.1. Topological Indices of Pandemic Trees

A pandemic tree is a complete R^0-ary tree, where R^0 is the reproduction number of a pandemic rounded to the nearest integer.

Definition 1 ([39]). *A k-ary tree is a rooted tree in which each node has no more than k children. All children of one node can be described as descendants of this node. In a k-ary tree, the maximum distance l from leaves to the root node is called the height of the k-ary tree. The root node is said to be at level 0. Inductively, the descendants of nodes at level i are at level* $i+1$, $0 \leq i \leq l-1$. *A k-ary tree is said to be a complete k-ary tree if each internal node has exactly k descendants. Thus, a pandemic tree is a complete k-ary tree, with the rounded epidemiological* R^0 *value of k. We denote this tree by* T_l^k, *where l is the height of the tree,* $k, l \geq 2$.

The number of vertices in level i, $0 \leq i \leq l$ of T_l^k is k^i. Hence, the total number of vertices and edges in T_l^k are $\frac{k^{l+1}-1}{k-1}$ and $\frac{k^{l+1}-1}{k-1} - 1$, respectively. The degree $d(v)$ of a vertex v in T_l^k is 1 , if v is a leaf; k, if v is the root and $k+1$, if v is an internal vertex. For illustration, the pandemic tree T_5^3 of level 5, and the pandemic tree T_6^6 of level 6 are shown in Figure 2a,b, respectively.

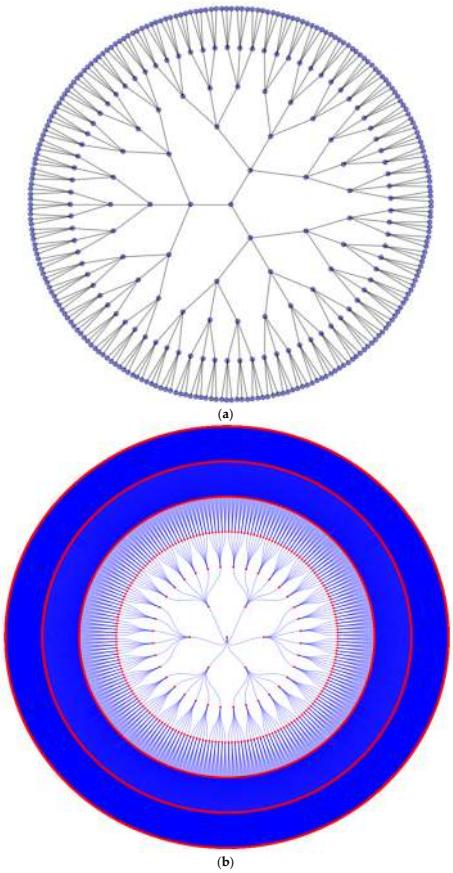

Figure 2. (**a**): A 5-level pandemic tree T_5^3, with reproduction number 3. (**b**): A 6-level pandemic tree T_6^6, with a reproduction number 6.

Theorem 1. *Let T_l^k denote a pandemic tree on l levels with a reproduction number k.*

Then:

(i) $GA_4\left(T_l^k\right) = \sum_{i=1}^{l} k^i \times \frac{2\sqrt{(l+i-1)(l+i)}}{2(l+i-1)+1}$;

(ii) $Zg_4\left(T_l^k\right) = \frac{k(k+2l-2lk+1)}{(k-1)^2} - \frac{k^{l+1}(k+4l-4lk+1)}{(k-1)^2}$;

(iii) $\Pi_4^*\left(T_l^k\right) = \prod_{i=1}^{l} (2(l+i)-1)^{k^i}$;

(iv) $Zg_6\left(T_l^k\right) = \frac{2k^{l+1}\left(2k^2l^2-lk^2-4kl^2+k+2l^2+l\right)}{(k-1)^3} - \frac{k\left(k^2l^2-lk^2-2kl^2+2k+l^2+l\right)}{(k-1)^3}$;

(v) $\Pi_6^*\left(T_l^k\right) = \prod_{i=1}^{l} ((l+i-1)(l+i))^{k^i}$;

(vi) $Zg_4\left(T_l^k, x\right) = \sum_{i=1}^{l} k^i \times x^{2(l+i-1)+1}$;

(vii) $Zg_6\left(T_l^k, x\right) = \sum_{i=1}^{l} k^i \times x^{(l+i-1)(l+i)}$;

(viii) $ABC_5\left(T_l^k\right) = \prod_{i=1}^{l} \left(\sqrt{\frac{2(l+i-1)-1}{(l+i-1)(l+i)}}\right)^{k^i}$;

(ix) $PI\left(T_l^k\right) = \frac{k\left(k^l-1\right)\left(k^{l+1}-1\right)}{(k-1)^2}$;

(x) $Sz\left(T_l^k\right) = \frac{k^{l+1}\left(2k-l-2k\times k^l+kl-kl\times k^l+k^{2+l}\times l\right)}{(k-1)^3}$.

Proof. We prove the results based on the edge partition and structure analysis of T_l^k :

- $E_{l+i-1,\,l+i} = \left\{e = uv \in E\left(T_l^k\right) \middle| ec(u) = l+i-1 \text{ and } ec(v) = l+i\right\}$ and $n_{l+i-1,l+i} = \left|E_{l+i-1,l+i}\right| = k^i$, where $i \in \{1,\ldots,l\}$:

and

- $E_{k+1,k} = \left\{e = uv \in E\left(T_l^k\right) \middle| d(u) = k+1 \text{ and } d(v) = k,\ n(u) = \left(\frac{k^l-1}{k-1}\right) \text{ and } n(v) = \left(\frac{k^{l+1}-1}{k-1}\right) - \left(\frac{k^l-1}{k-1}\right)\right\}$ and $n_{k+1,k} = \left|E_{k+1,k}\right| = k$;
- $E_{1,k+1} = \left\{e = uv \in E\left(T_l^k\right) \middle| d(u) = 1 \text{and} d(v) = k+1,\ n(u) = 1 \text{ and } n(v) = \left(\frac{k^{l+1}-1}{k-1}\right) - 1\right\}$ and $\left|E_{1,k}\right| = k^l$;
- $E_{k+1,k+1} = \left\{e = uv \in E\left(T_l^k\right) \middle| d(u) = d(v) = k+1, n(u) = \sum_{i=1}^{l-2}\left(\frac{k^{i+1}-1}{k-1}\right) \text{ and } n(v) = \left(\frac{k^{l+1}-1}{k-1}\right) - \sum_{i=1}^{l-2}\left(\frac{k^{i+1}-1}{k-1}\right)\right\}$ and $\left|E_{k,k}\right| = \sum_{i=1}^{l-2}(k^{l-i})$.

From the definitions we have:

$$GA_4\left(T_l^k\right) = \sum_{i=1}^{l} k^i \times \frac{2\sqrt{(l+i-1)(l+i)}}{2(l+i-1)+1};$$

$$Zg_4\left(T_l^k\right) = \sum_{i=1}^{l} k^i \times 2(l+i-1)+1 = \frac{k(k+2l-2lk+1)}{(k-1)^2} - \frac{k^{l+1}(k+4l-4lk+1)}{(k-1)^2};$$

$$\Pi_4^*\left(T_l^k\right) = \prod_{i=1}^{l}(2(l+i)-1)^{k^i};$$

$$Zg_6\left(T_l^k\right) = \sum_{i=1}^{l} k^i \times (l+i-1)(l+i)$$
$$= \frac{2k^{l+1}\left(2k^2l^2-lk^2-4kl^2+k+2l^2+l\right)}{(k-1)^3} - \frac{k\left(k^2l^2-lk^2-2kl^2+2k+l^2+l\right)}{(k-1)^3};$$

$$\Pi_6^*\left(T_l^k\right) = \prod_{i=1}^{l}((l+i-1)(l+i))^{k^i};$$

$$Zg_4\left(T_l^k,\, x\right) = \sum_{i=1}^{l} k^i \times x^{2(l+i-1)+1};$$

$$Zg_6\left(T_l^k,\, x\right) = \sum_{i=1}^{l} k^i \times x^{(l+i-1)(l+i)};$$

$$ABC_5\left(T_l^k\right) = \prod_{i=1}^{l}\left(\sqrt{\frac{2(l+i-1)-1}{(l+i-1)(l+i)}}\right)^{k^i}.$$

Further:

$$PI\left(T_l^k\right) = \left(\left(\frac{k^l-1}{k-1}\right) + \left(\left(\frac{k^{l+1}-1}{k-1}\right) - \left(\frac{k^l-1}{k-1}\right)\right)\right)\times k + \left(1 + \left(\left(\frac{k^{l+1}-1}{k-1}\right) - 1\right)\right) \times k^l$$
$$+ \sum_{i=1}^{l-2}(k^{l-i})\left\{\left(\frac{k^{i+1}-1}{k-1}\right) + \left(\left(\frac{k^{l+1}-1}{k-1}\right) - \left(\frac{k^{i+1}-1}{k-1}\right)\right)\right\}$$
$$= \frac{k\left(k^l-1\right)\left(k^{l+1}-1\right)}{(k-1)^2};$$

$$\begin{aligned} Sz\left(T_l^k\right) &= \left(\left(\tfrac{k^l-1}{k-1}\right)\times\left(\left(\tfrac{k^{l+1}-1}{k-1}\right)-\left(\tfrac{k^l-1}{k-1}\right)\right)\right)\times k+\left(1\times\left(\left(\tfrac{k^{l+1}-1}{k-1}\right)-1\right)\right)\times k^l \\ &+\sum_{i=1}^{l-2}(k^{l-i})\left\{\left(\tfrac{k^{i+1}-1}{k-1}\right)\times\left(\left(\tfrac{k^{l+1}-1}{k-1}\right)-\left(\tfrac{k^{i+1}-1}{k-1}\right)\right)\right\} \\ &= \frac{k^{l+1}\left(2k-l-2k\times k^l+kl-kl\times k^l+k^{2+l}\times l\right)}{(k-1)^3}. \end{aligned}$$

□

Theorem 2. *The various degree based topological indices of* T_l^k are given by:

(i) $M_1\left(T_l^k\right) = k^2+(k+1)^2\times\frac{k^l-k}{k-1}+k^l;$

(ii) $M_2\left(T_l^k\right) = k^l(k+1)+\frac{k^l-k^2}{k-1}(k+1)^2+k^2(k+1);$

(iii) $ABC\left(T_l^k\right) = k\sqrt{\frac{2k-1}{k(k+1)}}+k^l\sqrt{\frac{k}{k+1}}+\frac{k^l-k^2}{k-1}\times\frac{\sqrt{2k}}{k+1}.$

Proof. Let the vertex and edge sets of T_l^k be partitioned as follows:

- $P_1 = \left\{v\middle|\, d(v)=k\right\}$ and $|P_1|=1$;
- $P_2 = \{v|\, d(v)=k+1\}$ and $|P_2|=\frac{k^l-k}{k-1}$;
- $P_3 = \left\{v\middle|\, d(v)=1\right\}$ and $|P_3|=k^l$;

and

- $E_{k,k+1} = \left\{e=uv\in E\left(T_l^k\right)\middle|\, d(u)=k \text{ and } d(v)=k+1\right\}$ and $\left|E_{k,k+1}\right|=k$;
- $E_{1,k+1} = \left\{e=uv\in E\left(T_l^k\right)\middle|\, d(u)=1 \text{ and } d(v)=k+1\right\}$ and $\left|E_{1,k+1}\right|=k^l$;
- $E_{k+1,k+1} = \left\{e=uv\in E\left(T_l^k\right)\middle|\, d(u)=k+1 \text{ and } d(v)=k+1\right\}$ and $\left|E_{k+1,k+1}\right|=\sum_{i=2}^{l-1}k^i$.

By the definition of *first Zagreb index*, we have:

$$M_1\left(T_l^k\right) = \sum_{v\epsilon P_1}(d(v))^2+\sum_{v\epsilon P_2}(d(v))^2+\sum_{v\epsilon P_3}(d(v))^2 = k^2+(k+1)^2\times\frac{k^l-k}{k-1}+k^l.$$

From the definitions of M_2 and ABC we obtain:

$$\begin{aligned} M_2\left(T_l^k\right) &= \sum_{e\epsilon E_{k,k+1}}d(u)d(v)+\sum_{e\epsilon E_{1,k+1}}d(u)d(v)+\sum_{e\epsilon E_{k+1,k+1}}d(u)d(v) \\ &= ((k)(k+1))k+((1)(k+1))\,k^l+(k+1)(k+1)\,\tfrac{k^l-k^2}{2} \\ &= k^l(k+1)+\tfrac{k^l-k^2}{k-1}(k+1)^2+k^2(k+1); \\ ABC\left(T_l^k\right) &= k\sqrt{\tfrac{(k)+(k+1)-2}{(k)(k+1)}}+k^l\sqrt{\tfrac{(1)+(k+1)-2}{(1)(k+1)}} \\ &+\sum_{i=2}^{l-1}k^i\sqrt{\tfrac{(k+1)+(k+1)-2}{(k+1)(k+1)}} \\ &= k\sqrt{\tfrac{2k-1}{k(k+1)}}+k^l\sqrt{\tfrac{k}{k+1}}+\tfrac{k^l-k^2}{k-1}\times\tfrac{\sqrt{2k}}{k+1}. \end{aligned}$$

□

Remark 1. *The results obtained from Topo-Chemie-2020 [40] are shown in Table 1 for a comparison with the results obtained from Theorems 1 and 2.*

Table 1. Results obtained for the pandemic tree T_l^k with the computer code, compared with the results from the expressions in Theorems 1 and 2.

Index	Dimension *l*, *k*	From Expressions 1 and 2	Topo-Chemie-2020 [40]
$GA_4\left(T_l^k\right)$	$l = 3, k = 3$	38.8016	38.801700143357856
	$l = 3, k = 4$	83.5947	83.59488962413361
	$l = 4, k = 3$	119.6838	119.6839561076481
	$l = 4, k = 4$	339.1496	339.1498266447425
$Zg_4\left(T_l^k\right)$	$l = 3, k = 3$	399	399
	$l = 3, k = 4$	876	876
	$l = 4, k = 3$	1692	1692
	$l = 4, k = 4$	4884	4884
$\Pi_4^*\left(T_l^k\right)$	$l = 3, k = 3$	$1.74212456 \times 10^{39}$	$1.742124563637115 \times 10^{39}$
	$l = 3, k = 4$	$1.98337192 \times 10^{85}$	$1.9833719240465464 \times 10^{85}$
	$l = 4, k = 3$	$3.75944893 \times 10^{137}$	$3.7594489384955 63 \times 10^{137}$
	$l = 4, k = 4$	Infinity	+Inf
$Zg_6\left(T_l^k\right)$	$l = 3, k = 3$	1026	1026
	$l = 3, k = 4$	2288	2288
	$l = 4, k = 3$	6000	6000
	$l = 4, k = 4$	17,584	17,584
$\Pi_6^*\left(T_l^k\right)$	$l = 3, k = 3$	$6.74664061 \times 10^{54}$	$6.746640616477462 \times 10^{54}$
	$l = 3, k = 4$	$4.66622007 \times 10^{119}$	$4.666220065428966 \times 10^{119}$
	$l = 4, k = 3$	$4.24758724 \times 10^{202}$	$4.247587242244764 \times 10^{202}$
	$l = 4, k = 4$	Infinity	+Inf
$ABC_5\Pi\left(T_l^k\right)$	$l = 3, k = 3$	$2.0850970590 \times 10^{-10}$	$2.0850970590395853 \times 10^{-10}$
	$l = 3, k = 4$	$7.2443933360 \times 10^{-22}$	$7.2443933361227945 \times 10^{-22}$
	$l = 4, k = 3$	$2.6373891592 \times 10^{-37}$	$2.6373891591075294 \times 10^{-37}$
	$l = 4, k = 4$	$1.26583295 \times 10^{-105}$	$1.2658329528339406 \times 10^{-105}$
$PI\left(T_l^k\right)$	$l = 3, k = 3$	1560	1560
	$l = 3, k = 4$	7140	7140
	$l = 4, k = 3$	14,520	14,520
	$l = 4, k = 4$	115,940	115,940
$Sz\left(T_l^k\right)$	$l = 3, k = 3$	3402	3402
	$l = 3, k = 4$	17,152	17,152
	$l = 4, k = 3$	44,712	44,712
	$l = 4, k = 4$	389,120	389,120
$M_1\left(T_l^k\right)$	$l = 3, k = 3$	228	228
	$l = 3, k = 4$	580	580
	$l = 4, k = 3$	714	714
	$l = 4, k = 4$	2372	2372
$M_2\left(T_l^k\right)$	$l = 3, k = 3$	288	288
	$l = 3, k = 4$	800	800
	$l = 4, k = 3$	936	936
	$l = 4, k = 4$	3360	3360
$ABC\left(T_l^k\right)$	$l = 3, k = 3$	30.8308	30.83052949654569
	$l = 3, k = 4$	68.6607	68.66073893642222
	$l = 4, k = 3$	94.13	94.12995706469174
	$l = 4, k = 4$	276.5956	276.59462680515827

3.2. Topological Indices of Cayley Trees

Definition 2. *A tree is said to be a k-Cayley tree with l levels, denoted by C(k, l), k, $l \geq 3$ if all vertices have the same degree k except the leaves [41]. The number of vertices and edges in C(k, l) are $\frac{k(k-1)^l-2}{k-2}$ and $\frac{k(k-1)^l-2}{k-2}-1$, respectively. For illustration, the Cayley trees C(3,6) and C(6,6) are shown in Figure 3a,b, respectively.*

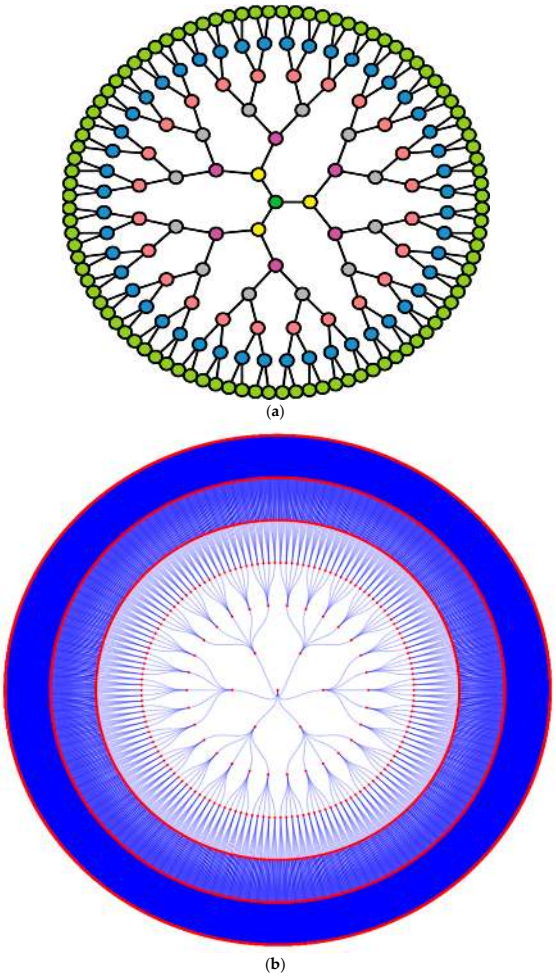

Figure 3. (**a**): A 3-Cayley tree, C(3,6), of degree 3 with 6 levels. (**b**): A 6-Cayley tree, C(6,6), of degree 6 with 6 levels.

Theorem 3. *For a Cayley tree $C(k,l)$, with $k,\ l \geq 3$, we obtai*:

(i) $GA_4(C(k,l)) = \sum_{i=1}^{l} k(k-1)^{i-1} \times \frac{2\sqrt{(l+i-1)(l+i)}}{2(l+i-1)+1}$;

(ii) $Zg_4(C(k,l)) = \frac{(k(4l+k-2lk-8l(k-1)^l-k(k-1)^l+4lk(k-1)^l))}{(k-2)^2}$;

(iii) $\Pi_4^*(C(k,l)) = \prod_{i=1}^{l} (2(l+i)-1)^{k(k-1)^{i-1}}$;

(iv) $Zg_6(C(k,l)) = k\left(\left(\frac{4l^2k-l^2k^2-4l^2+lk^2-2lk-2k+2}{(k-2)^3}\right)+\left(\frac{2(k-1)^l(2l^2k^2-8l^2k+8l^2-lk^2+2lk+k-1)}{(k-2)^3}\right)\right)$;

(v) $\Pi_6^*(C(k,l)) = \prod_{i=1}^{l} ((l+i-1)(l+i))^{k(k-1)^{i-1}}$;

(vi) $Zg_4(C(k,l),\ x) = \sum_{i=1}^{l} k(k-1)^{i-1} \times x^{2(l+i-1)+1}$;

(vii) $Zg_6(C(k,l),\ x) = \sum_{i=1}^{l} k(k-1)^{i-1} \times x^{(l+i-1)(l+i)}$;

(viii) $ABC_5(C(k,l)) = \prod_{i=1}^{l}\left(\sqrt{\frac{2(l+i-1)-1}{(l+i-1)(l+i)}}\right)^{k(k-1)^{i-1}}$;

(ix) $PI(C(k,l)) = \frac{\left(k\left(k(k-1)^l-2\right)\left((k-1)^l-1\right)\right)}{(k-2)^2}$;

(x) $Sz(C(k,l)) = \frac{\left(k\left(2k(k-1)^l-2k(k-1)^{2l}+(k-1)^{2l}-2kl(k-1)^{2l}+lk^2(k-1)^{2l}-1\right)\right)}{(k-2)^3}$.

Proof. We compute the edge partition with respect to eccentricities and the edge partitions with respect to the degrees of the associated vertices from the edge set of $C(k,\ l)$ as follows:

- $E_{l+i-1,\ l+i} = \{e = uv \in E(C(k,l)) \big| ec(u) = l+i-1 \text{ and } ec(v) = l+i\}$ and $n_{l+i-1,\ l+i} = \left|E_{l+i-1,\ l+i}\right| = k(k-1)^{i-1}$, where $i \in \{1,\ldots,l\}$:

and

- $E_{k,k} = \left\{e = uv \in E(C(k,l)) \middle| d(u) = d(v) = k,\ n(u) = \left(\frac{(k-1)^l-1}{k-2}\right) \text{and } n(v) = \left(\frac{k(k-1)^l-(k-1)^l-1}{k-2}\right)\right\}$ and $\left|E_{k,k}\right| = k$;
- $E_{1,k} = \left\{e = uv \in E(C(k,l)) \middle| d(u) = 1 \text{ and } d(v) = k,\ n(u) = 1 \text{ and } n(v) = \left(\frac{k(k-1)^l-2}{k-2} - 1\right)\right\}$ and $\left|E_{1,k}\right| = k(k-1)^{l-1}$;
- $E_{k,k} = \left\{e = uv \in E(C(k,l)) \middle| d(u) = d(v) = k, n(u) = \sum_{i=1}^{l-2}\left(\frac{(k-1)^{i+1}-1}{k-2}\right) \text{and } n(v) = \sum_{i=1}^{l-2}\left(\frac{k(k-1)^d-2}{k-2} - \frac{(k-1)^{i+1}-1}{k-2}\right)\right\}$ and $\left|E_{k,k}\right| = \sum_{i=1}^{l-2} k(k-1)^{l-i-1}$.

From the definitions of the eccentric version indices, we obtain:

$$GA_4(C(k,l)) = \sum_{i=1}^{l} k(k-1)^{i-1} \times \frac{2\sqrt{(l+i-1)(l+i)}}{2(l+i-1)+1};$$

$$Zg_4(C(k,l)) = \frac{\left(k\left(4l+k-2lk-8l(k-1)^l-k\left(k-1\right)^l+4lk\left(k-1\right)^l\right)\right)}{(k-2)^2};$$

$$\Pi_4^*(C(k,l)) = \prod_{i=1}^{l}(2(l+i)-1)^{k(k-1)^{i-1}};$$

$$\begin{aligned} Zg_6(C(k,l)) &= k\left(\left(\frac{4l^2k-l^2k^2-4l^2+lk^2-2lk-2k+2}{(k-2)^3}\right)\right. \\ &\quad \left.+\left(\frac{2(k-1)^l(2l^2k^2-8l^2k+8l^2-lk^2+2lk+k-1}{(k-2)^3}\right)\right); \end{aligned}$$

$$\Pi_6^*(C(k,l)) = \prod_{i=1}^{l}((l+i-1)(l+i))^{k(k-1)^{i-1}};$$

$$Zg_4(C(k,l),\ x) = \sum_{i=1}^{l} k(k-1)^{i-1} \times x^{2(l+i-1)+1};$$

$$Zg_6(C(k,l),\ x) = \sum_{i=1}^{l} k(k-1)^{i-1} \times x^{(l+i-1)(l+i)};$$

$$ABC_5(C(k,l)) = \prod_{i=1}^{l}\left(\sqrt{\frac{2(l+i-1)-1}{(l+i-1)(l+i)}}\right)^{k(k-1)^{i-1}}.$$

By the definitions of the PI and Sz indices we have:

$$\begin{aligned} PI(C(k,l)) &= \left(\left(\tfrac{(k-1)^l-1}{k-2}\right)+\left(\tfrac{k(k-1)^l-(k-1)^l-1}{k-2}\right)\right)\times k+\left(1+\left(\tfrac{k(k-1)^l-2}{k-2}-1\right)\right)\times \\ &\quad k(k-1)^{l-1} \\ &\quad +\sum_{i=1}^{l-2} k(k-1)^{l-i-1}\left\{\left(\tfrac{(k-1)^{i+1}-1}{k-2}\right)+\left(\left(\tfrac{k(k-1)^l-2}{k-2}\right)-\left(\tfrac{(k-1)^{i+1}-1}{k-2}\right)\right)\right\} \\ &= \tfrac{\left(k\left(k(k-1)^l-2\right)\left((k-1)^l-1\right)\right)}{(k-2)^2}; \end{aligned}$$

$$\begin{aligned} Sz(C(k,l)) &= \left(\left(\tfrac{(k-1)^l-1}{k-2}\right)\times\left(\tfrac{k(k-1)^l-(k-1)^l-1}{k-2}\right)\right)\times k+\left(1\times\left(\tfrac{k(k-1)^l-2}{k-2}-1\right)\right)\times \\ &\quad k(k-1)^{l-1} \\ &\quad +\sum_{i=1}^{l-2} k(k-1)^{l-i-1}\left\{\left(\tfrac{(k-1)^{i+1}-1}{k-2}\right)\times\left(\left(\tfrac{k(k-1)^l-2}{k-2}\right)-\left(\tfrac{(k-1)^{i+1}-1}{k-2}\right)\right)\right\} \\ &= \tfrac{\left(k\left(2k(k-1)^l-2k(k-1)^{2l}+(k-1)^{2l}-2kl(k-1)^{2l}+lk^2(k-1)^{2l}-1\right)\right)}{(k-2)^3}. \end{aligned}$$

□

Theorem 4. *The various degree based topological indices of $C(k,l)$ are given by:*

(i) $M_1(C(k,l)) = \frac{k(k(k-1)^l-2k+2(k-1)^l}{k-2}$;

(ii) $M_2(C(k,l)) = \frac{k^2(2\left(k-1\right)^l-k)}{k-2}$;

(iii) $ABC(C(k,l)) = \left(\frac{k(k-1)^l-k+1}{k^2-3k+2}\right)\frac{\sqrt{2(k-1)}}{k}+k(k-1)^{l-1}\sqrt{\frac{k-1}{k}}$.

Proof. Partition the vertex and edge sets of $C(k,l)$ as follows:

- $P_1 = \left\{v\middle|\, d(v)=k\right\}$ and $|P_1| = \left(\frac{k(k-1)^{l-1}-2}{k-2}\right)$;
- $P_2 = \left\{v\middle|\, d(v)=1\right\}$ and $|P_2| = k(k-1)^{l-1}$:

and

- $E_{k,k} = \left\{e=uv\in E(C(k,l))\middle|\, d(u)=k \text{ and } d(v)=k\right\}$ and $\left|E_{k,k}\right| = \left(\frac{k(k-1)^l-k+1}{k^2-3k+2}\right)$;
- $E_{1,k} = \left\{e=uv\in E(C(k,l))\middle|\, d(u)=1 \text{ and } d(v)=k\right\}$ and $\left|E_{1,k}\right| = k(k-1)^{l-1}$.

By the definition of M_1:

$$\begin{aligned} M_1(C(k,l)) &= \sum_{v\epsilon P_1}(d(v))^2+\sum_{v\epsilon P_2}(d(v))^2 \\ &= k^2\left(\tfrac{k(k-1)^{l-1}-2}{k-2}\right)+\left(k(k-1)^{l-1}\right)\times 1 \\ &= \tfrac{k(k(k-1)^l-2k+2(k-1)^l}{k-2}. \end{aligned}$$

Again, by the definitions of M_2 and ABC we obtain:

$$\begin{aligned} M_2(C(k,l)) &= \sum_{e\epsilon E_{k,k}} d(u)d(v)+\sum_{e\epsilon E_{1,k}} d(u)d(v) \\ &= (k\times k)\left(\tfrac{k(k-1)^l-k+1}{k^2-3k+2}\right)+(k\times 1)\left(k(k-1)^{l-1}\right) \\ &= \tfrac{k^2(2\left(k-1\right)^l-k)}{k-2}; \end{aligned}$$

$$\begin{aligned} ABC(C(k,l)) &= \sum_{e\epsilon E_{k,k}} \sqrt{\tfrac{d(u)+d(v)-2}{d(u)d(v)}} + \sum_{e\epsilon E_{1,k}} \sqrt{\tfrac{d(u)+d(v)-2}{d(u)d(v)}} \\ &= \left(\tfrac{k(k-1)^l-k+1}{k^2-3k+2}\right)\sqrt{\tfrac{(k)+(k)-2}{(k)(k)}} + k(k-1)^{l-1}\sqrt{\tfrac{(1)+(k)-2}{(1)(k)}} \\ &= \left(\tfrac{k(k-1)^l-k+1}{k^2-3k+2}\right)\tfrac{\sqrt{2(k-1)}}{k} + k(k-1)^{l-1}\sqrt{\tfrac{k-1}{k}}. \end{aligned}$$

□

Remark 2. *The results obtained from Topo-Chemie-2020 [40] shown in Table 2 corroborate with the results obtained from Theorems 3 and 4.*

Table 2. Results obtained for the Cayley Trees $C(k,l)$ with the computer code, compared with the results from the expressions in Theorems 3 and 4.

Index	Dimension *k, l*	Expressions 3 and 4	Topo-Chemie-2020 [40]
$GA_4\ (C(k,l))$	$k=3, l=3$	20.8823882414	20.88238824139906
	$k=3, l=4$	44.8676307844	44.86763078442802
	$k=4, l=3$	51.7356001911	51.73560019114378
	$k=4, l=4$	159.578608144	159.57860814353083
$Zg_4\ (C(k,l))$	$k=3, l=3$	207	207
	$k=3, l=4$	609	609
	$k=4, l=3$	532	532
	$k=4, l=4$	2256	2256
$\Pi_4^*(C(k,l))$	$k=3, l=3$	$5.72086104 \times 10^{20}$	$5.7208610362887386 \times 10^{20}$
	$k=3, l=4$	$5.06517068 \times 10^{50}$	$5.065170680143067 \times 10^{50}$
	$k=4, l=3$	$2.09623003 \times 10^{52}$	$2.0962300336315637 \times 10^{52}$
	$k=4, l=4$	$2.71330692 \times 10^{183}$	$2.7133069091840815 \times 10^{183}$
$Zg_6\ (C(k,l))$	$k=3, l=3$	516	516
	$k=3, l=4$	2088	2088
	$k=4, l=3$	1368	1368
	$k=4, l=4$	8000	8000
$\Pi_6^*(C(k,l))$	$k=3, l=3$	$5.87731231 \times 10^{28}$	$5.877312307199999 \times 10^{28}$
	$k=3, l=4$	1.5897237×10^{74}	$1.589723697730939 \times 10^{74}$
	$k=4, l=3$	$1.27482362 \times 10^{73}$	$1.2748236216396078 \times 10^{73}$
	$k=4, l=4$	1.482028×10^{270}	$1.4820280048671849 \times 10^{270}$
$ABC_5\Pi\ (C(k,l))$	$k=3, l=3$	0.00000840649	0.000008406491899037542
	$k=3, l=4$	$4.4189082 \times 10^{-14}$	$4.419672639996076 \times 10^{-14}$
	$k=4, l=3$	$1.23642668 \times 10^{-13}$	$1.2364266794260217 \times 10^{-13}$
	$k=4, l=4$	$1.66132298 \times 10^{-49}$	$1.6913453312569212 \times 10^{-49}$
$PI(C(k,l))$	$k=3, l=3$	462	462
	$k=3, l=4$	2070	2070
	$k=4, l=3$	2756	2756
	$k=4, l=4$	25,760	25,760

Table 2. *Cont.*

Index	Dimension k, l	Expressions 3 and 4	Topo-Chemie-2020 [40]
$M_1(C(k,l))$	$k=3, l=3$	102	102
	$k=3, l=4$	222	222
	$k=4, l=3$	308	308
	$k=4, l=4$	956	956
$M_2(C(k,l))$	$k=3, l=3$	117	117
	$k=3, l=4$	261	261
	$k=4, l=3$	400	400
	$k=4, l=4$	1264	1264
$ABC(C(k,l))$	$k=3, l=3$	15.7979589714	15.797958971132715
	$k=3, l=4$	33.5959179422	33.59591794226542
	$k=4, l=3$	40.9748735074	40.974873507372514
	$k=4, l=4$	125.374110265	125.37411026490041

Remark 3. *Gutman et al. [42] proved that the Szeged index and the Wiener index are equal for trees. Hence, in particular, W and Sz indices are equal for the pandemic and Cayley trees.*

3.3. Christmas Tree Network

Definition 3 ([43]). *For $s \geq 2$, a Christmas tree $CT(s)$ is composed of an s^{th} slim tree $ST(s) = (V_1, E_1, u_1, l_1, r_1)$ and an $(s+1)^{th}$ slim tree $ST(s+1) = (V_2, E_2, u_2, l_2, r_2)$ together with the edges (u_1, u_2), (l_1, r_2), and (l_2, r_1), where $ST(s) = (V, E, u, l, r)$, with V as the node set, E as the edge set, $u \in V$ as the root node, $l \in V$ as the left node, and $r \in V$ as the right node defined below:*

1 *$ST(2)$ is the complete graph K_3 with its nodes labelled with u, l and r.*
2 *The s^{th} slim tree $ST(s)$, with $s \geq 3$, is composed of a root node u and two disjoint copies of $(s-1)^{th}$ slim trees as the left subtree and right subtree, denoted by $ST^l(s-1) = (V_1, E_1, u_1, l_1, r_1)$ and $ST^r(s-1) = (V_2, E_2, u_2, l_2, r_2)$, respectively and $ST(s) = (V, E, u, l, r)$ is given by $V = V_1 \cup V_2 \cup \{u\}$, $E = E_1 \cup E_2 \cup \{(u, u_1), (u, u_2), (r_1, l_2)\}$, $l = l_1$, $r = r_2$.*

For illustration, the Christmas tree $CT(3)$ is shown in Figure 4. The number of nodes and edges of $CT(s)$ are $(3 \times 2^s) - 2$ and $\frac{9 \times 2^s - 6}{2}$, respectively.

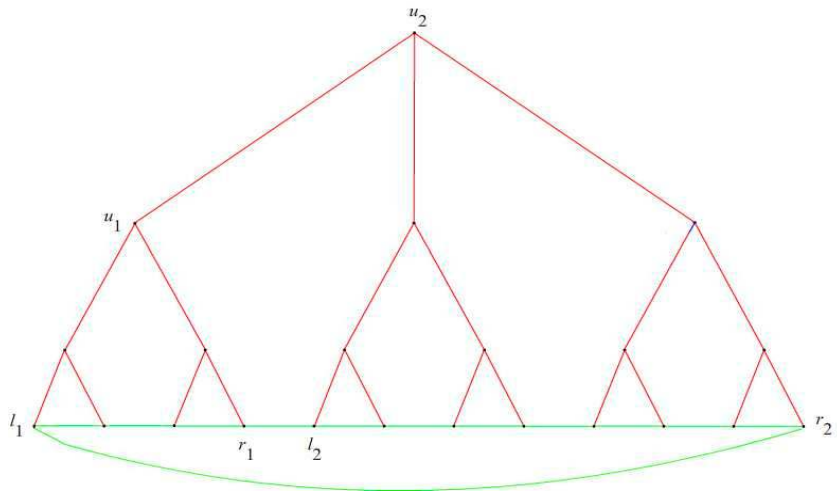

Figure 4. A Christmas tree $CT(3)$ with 3 levels.

Theorem 5. *We have the following results for CT(s):*

(i) $GA_4(CT(s)) = \sum_{i=1}^{s} 3\left(2^{i-1}\right)\frac{2\sqrt{(s+i-1)(s+i)}}{2(s+i-1)+1} + 3\left(2^{s-1}\right)$;

(ii) $Zg_4(CT(s)) = 12s(2^s) - 6s - 9(2^s) + 9 + 12s\left(2^{s-1}\right)$;

(iii) $\Pi_4^*(CT(s)) = (4s)^{3(2^{s-1})} \prod_{i=1}^{s} (2(s+i)-1)^{3(2^{i-1})}$;

(iv) $Zg_6(CT(s)) = 9s + s^2\left(12 \times 2^{s-1} - 3\right) + 3 \times 2^{s+1}\left(2s^2 - 3s + 2\right) - 12$;

(v) $\Pi_6^*(CT(s)) = \left(4s^2\right)^{3(2^{s-1})} \prod_{i=1}^{s} ((s+i-1)(s+i))^{3(2^{i-1})}$;

(vi) $Zg_4(CT(s),\, x) = \sum_{i=1}^{s} 3\left(2^{i-1}\right)x^{2(s+i)-1} + 3\left(2^{s-1}\right)x^{4s}$;

(vii) $Zg_6(CT(s),\, x) = \sum_{i=1}^{s} 3\left(2^{i-1}\right)x^{(s+i-1)(s+i)} + 3\left(2^{s-1}\right)x^{4s^2}$;

(viii) $ABC_5\Pi(CT(s)) = \prod_{i=1}^{s}\left(\frac{2(s+i)-3}{(s+i-1)(s+i)}\right)^{3(2^{i-2})} \times \left(\frac{4s-2}{4s^2}\right)^{3(2^{s-2})}$.

Proof. The edge partitions of $CT(s)$ are defined below:

- $E_{s+i-1,\, s+i} = \{e = uv \in E(CT(s)) \big| ec(u) = s+i-1 \text{ and } ec(v) = s+i\}$ and $n_{s+i-1,s+i} = \left|E_{s+i-1,s+i}\right| = 3(2^{i-1})$, where $i \in \{1, \ldots, s\}$;
- $E_{2s,\, 2s} = \{e = uv \in E(CT(s)) \big| ec(u) = ec(v) = 2s\}$ and $n_{2s,\, 2s} = \left|E_{2s,\, 2s}\right| = 3(2^{s-1})$.

Computations similar to those of Theorems 1 and 3 yield the following results. □

Theorem 6. *The various degree based topological indices of CT(s) are given by:*

(i) $M_1\,(CT(s)) = 9(3 \times 2^s - 2)$;

(ii) $M_2\,(CT(s)) = 9\left(\frac{9\times 2^s - 6}{2}\right)$;

(iii) $ABC(CT(s)) = (3 \times 2^s - 2)$.

Proof. As $CT(s)$ is 3-regular, it is enough to consider the following partitions:

- $P_1 = \left\{v \middle| \, d(v) = 3\right\}$ and $|P_1| = (3.2^s - 2)$:

and

- $E_{3,3} = \{e = uv \in E(CT(s)) \,\big|d(u) = \, d(v) = 3\}$ and $\left|E_{3,3}\right| = \frac{(9\times 2^s - 6)}{2}$.

A direct application of the definitions yields the required results. □

Remark 4. *The results obtained from Topo-Chemie-2020 [40] are shown in Table 3 for a comparison with the results obtained from Theorems 5 and 6.*

Table 3. Results obtained for the Christmas trees, $CT(s)$ with the computer code, compared with the results from the expressions in Theorems 5 and 6.

Index	Dimensions	From Expressions 5 and 6	Topo-Chemie-2020 [40]
$GA_4\,(CT(s))$	$s = 3$	32.8823	32.882388241399056
	$s = 4$	68.8671	68.86763078442803
	$s = 5$	140.8350	140.83501683597572
$Zg_4\,(CT(s))$	$s = 3$	351	351
	$s = 4$	993	993
	$s = 5$	2571	2571

Table 3. *Cont.*

Index	Dimensions	From Expressions 5 and 6	Topo-Chemie-2020 [40]
$\Pi_4^*(CT(s))$	$s = 3$	$5.10073079 \times 10^{33}$	$5.10077716500643 \times 10^{33}$
	$s = 4$	$4.01304165 \times 10^{79}$	$4.0130416580886176 \times 10^{79}$
	$s = 5$	$1.91126114 \times 10^{177}$	$1.9112611351919165 \times 10^{177}$
$Zg_6\,(CT(s))$	$s = 3$	948	948
	$s = 4$	3624	3624
	$s = 5$	11,862	11,862
$\Pi_6^*(CT(s))$	$s = 3$	2.7848947×10^{47}	$2.7848946955924445 \times 10^{47}$
	$s = 4$	$3.54520226 \times 10^{117}$	$3.5452023119163584 \times 10^{117}$
	$s = 5$	$3.37859549 \times 10^{269}$	$3.3785954904846475 \times 10^{269}$
$ABC_5\Pi\,(CT(s))$	$s = 3$	$3.8618890813 \times 10^{-9}$	$3.861889064427591 \times 10^{-9}$
	$s = 4$	$5.3059950832 \times 10^{-22}$	$5.305995082939164 \times 10^{-22}$
	$s = 5$	$1.7589082206 \times 10^{-50}$	$1.7589082206095107 \times 10^{-50}$
$M_1(CT(s))$	$s = 3$	198	198
	$s = 4$	414	414
	$s = 5$	846	846
$M_2(CT(s))$	$s = 3$	297	297
	$s = 4$	621	621
	$s = 5$	1269	1269
$ABC(CT(s))$	$s = 3$	22	22.000000000000004
	$s = 4$	46	45.99999999999997
	$s = 5$	94	94.00000000000011

3.4. Corona Product of Christmas Tree and a Path

Graph operations facilitate decomposition of a graph G into two or more isomorphic subgraphs. The corona product $G_1 \Theta G_2$ of two graphs G_1 (with n_1 vertices and m_1 edges) and G_2 (with n_2 vertices and m_2 edges) is defined as the graph obtained by taking a copy of G_1 and n_1 copies of G_2, and then joining the i^{th} vertex of G_1 with edges to every vertex in the i^{th} copy of G_2. It follows from the definition of the corona product that $G_1 \Theta G_2$ has $n_1 + n_1 n_2$ vertices and $m_1 + n_1 m_2 + n_1 n_2$ edges. It is easy to see that $G_1 \Theta G_2$ is not in general isomorphic to $G_2 \Theta G_1$ [44].

The corona product $CT(3) \Theta P_3$ is shown in Figure 5. The number of nodes and edges of $CT(s) \Theta P_n$ are $3 \times 2^s - 2 + (3 \times 2^s - 2)n$ and $\frac{9 \times 2^s - 6}{2} + ((3 \times 2^s) - 2)(2n - 1)$, respectively. The eccentricity-based topological indices for $CT(s) \Theta P_n$, $s, n \geq 2$ are given in Theorem 7.

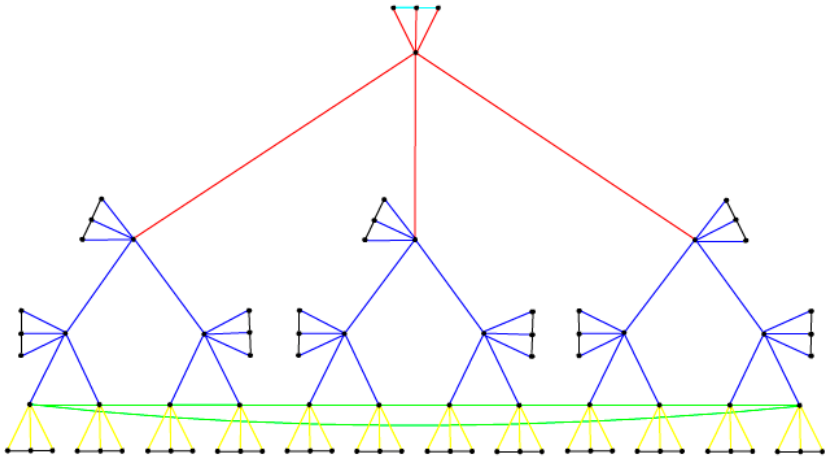

Figure 5. The corona product $CT(3) \Theta P_3$ of a Christmas tree $CT(3)$ and a path P_3.

Theorem 7. *For $s, n \geq 2$, we have the following for $CT(s)\Theta P_n$:*

(i) $GA_4(CT(s)\Theta P_n) = (6+2n)\frac{\sqrt{(s+1)(s+2)}}{2s+3} + \sum_{i=2}^{s} 3\left(2^{i-2}\right)(2+n)\frac{2\sqrt{(s+i)(s+i+1)}}{2(s+i)+1}$
$+6n\left(2^{s-1}\right)\frac{\sqrt{(2s+1)(2s+2)}}{4s+3} + \sum_{i=1}^{s} 3\left(2^{i-1}\right)(n-1)\frac{2(s+i+2)}{2(s+i+1)+2} + 3\left(2^{s-1}\right) + n - 1;$

(ii) $Zg_4(CT(s)\Theta P_n) = n(9\times 2^s - 2 + 24s\times 2^s) + s(6\times 2^s - 8n - 2) - 6\times 2^s + 5;$

(iii) $\Pi_4^*(CT(s)\Theta P_n) = (2s+3)^{3+n} \times \prod_{i=2}^{s}(2(s+i)+1)^{(6+3n)2^{i-2}} \times (4s+3)^{3n(2^{s-1})}$
$\times \prod_{i=1}^{s}(2(s+i+2))^{(3n-3)2^{i-1}} \times (4s+2)^{3(2^{s-1})} \times (2s+4)^{n-1};$

(iv) $Zg_6(CT(s)\Theta P_n) = s^2(6\times 2^s - 4n + 24n\times 2^s - 1) + s(5 - 2n - 12\times 2^s + 18n\times 2^s) + 2^s\left(15n - \frac{3}{2}\right) - 9n - 1;$

(v) $\Pi_6^*(CT(s)\Theta P_n) = \left(s^2+3s+2\right)^{3+n} \times \prod_{i=2}^{s}((s+i)(s+i+1))^{(6+3n)2^{i-2}} \times\left(2\left(2s^2+3s+1\right)\right)^{3n(2^{s-1})} \times$
$\prod_{i=1}^{s}(s+i+2)^{(3n-3)2^i} \times (2s+1)^{6(2^{s-1})} \times (s+2)^{2(n-1)};$

(vi) $Zg_4(CT(s)\Theta P_n, x) = (3+n)x^{2s+3} + (6+3n)\sum_{i=2}^{s} 2^{i-2}x^{2(s+i)+1} + 3n\left(2^{s-1}\right)x^{4s+3}$
$+3(n-1)\sum_{i=1}^{s} 2^{i-1}x^{2(s+i+2)} + 3\left(2^{s-1}\right)x^{4s+2} + (n-1)x^{2(s+2)};$

(vii) $Zg_6(CT(s)\Theta P_n, x) = (3+n)x^{s^2+3s+2} + (6+3n)\sum_{i=2}^{s} 2^{i-2}x^{(s+i)(s+i+1)} + 3n\left(2^{s-1}\right)x^{(2s+1)(2s+2)} +$
$3(n-1)\sum_{i=1}^{s} 2^{i-1}x^{(s+i+2)^2} + 3\left(2^{s-1}\right)x^{(2s+1)^2} + (n-1)x^{(s+2)^2};$

(viii) $ABC_5\Pi(CT(s)\Theta P_n) = \left(\sqrt{\frac{2s+1}{(s+1)(s+2)}}\right)^{3+n} \times \prod_{i=2}^{s}\left(\frac{2(s+i)-1}{(s+i+1)(s+i)}\right)^{(6+3n)(2^{i-3})} \times\left(\frac{4s+1}{(2s+1)(2s+2)}\right)^{3n(2^{s-2})} \times$
$\prod_{i=1}^{s}\left(\frac{2(s+i+1)}{(s+i+2)^2}\right)^{(3n-3)(2^{i-2})} \times\left(\frac{\sqrt{4s}}{(2s+1)}\right)^{3(2^{s-1})} \times\left(\frac{\sqrt{2(s+1)}}{s+2}\right)^{n-1}.$

Proof. In $CT(s)\Theta P_n$, we have the following partitions:

- $E_{s+1,\,s+2} = \{e = uv \in E(CT(s)\Theta P_n)\,|ec(u) = s+1 \text{ and } ec(v) = s+2\}$ and $n_{s+1,\,s+2} = |E_{s+1,\,s+2}| = 3+n$;
- $E_{s+i,\,s+i+1} = \{e = uv \in E(CT(s)\Theta P_n)\,|ec(u) = s+i \text{ and } ec(v) = s+i+1\}$ and $n_{s+i,\,s+i+1} = |E_{s+i,\,s+i+1}| = 3(2^{i-2})(2+n)$, where $i \in \{2,\ldots,s\}$;
- $E_{2s+1,\,2s+2} = \{e = uv \in E(CT(s)\Theta P_n)\,|ec(u) = 2s+1 \text{ and } ec(v) = 2s+2\}$ and $n_{2s+1,\,2s+2} = |E_{2s+1,\,2s+2}| = 3n(2^{s-1})$;
- $E_{s+i+2,\,s+i+2} = \{e = uv \in E(CT(s)\Theta P_n)\,|ec(u) = ec(v) = s+i+2\}$ and $n_{s+i+2,\,s+i+2} = |E_{s+i+2,\,s+i+2}| = 3(2^{i-1})(n-1)$, where $i \in \{1,\ldots,s\}$;
- $E_{2s+1,\,2s+1} = \{e = uv \in E(CT(s)\Theta P_n)\,|ec(u) = ec(v) = 2s+1\}$ and $n_{2s+1,\,2s+1} = |E_{2s+1,\,2s+1}| = 3(2^{s-1})$;
- $E_{s+2,\,s+2} = \{e = uv \in E(CT(s)\Theta P_n)\,|ec(u) = ec(v) = s+2\}$ and $n_{s+2,\,s+2} = |E_{s+2,\,s+2}| = n-1$.

Let the edge colors red, blue, yellow, black, green, and sky blue in Figure 5 represent the edge partitions $E_{3+1,\,3+2}$, $E_{s+i,\,s+i+1}$, $E_{6+1,\,6+2}$, $E_{s+i+2,\,s+i+2}$, $E_{6+1,\,6+1}$, and $E_{3+2,\,3+2}$, respectively. Hence, the edge partitions of $CT(3)\ \Theta P_3$ are given as follows:

- $E_{3+1,\,3+2} = \{e = uv \in E(CT(3)\Theta P_3)\,|ec(u) = 3+1 \textit{ and } ec(v) = 3+2\}$ and $n_{3+1,\,3+2} = n_{4,5} = |E_{4,\,5}| = 3+3 = 6$;
- $E_{s+i,\,s+i+1} = \{e = uv \in E(CT(3)\Theta P_3)\,|ec(u) = s+i \text{ and } ec(v) = s+i+1\}$ and $n_{s+i,\,s+i+1} = |E_{s+i,\,s+i+1}| = 3(2^{i-2})(2+3) = 15\left(2^{i-2}\right)$, where $i \in \{2,3\}$;
- $E_{6+1,\,6+2} = \{e = uv \in E(CT(3)\Theta P_3)\,|ec(u) = 6+1 \text{ and } ec(v) = 6+2\}$ and $n_{6+1,\,6+2} = n_{7,8} = |E_{7,\,8}| = 3(3(2^{3-1})) = 36$;

- $E_{s+i+2,\,s+i+2} = \{e = uv \in E(CT(3)\Theta P_3)\big|ec(u) = ec(v) = s+i+2\}$ and $n_{s+i+2,\,s+i+2} = \left|E_{s+i+2,\,s+i+2}\right| = 3(2^{i-1})(n-1)$, where $i \in \{1,2,3\}$;
- $E_{6+1,\,6+1} = \{e = uv \in E(CT(3)\Theta P_3)\big|ec(u) = ec(v) = 6+1\}$ and $n_{7,7} = \left|E_{7,7}\right| = 3(2^{3-1}) = 12$;
- $E_{3+2,\,3+2} = \{e = uv \in E(CT(3)\Theta P_3)\big|ec(u) = ec(v) = 3+2\}$ and $n_{3+2,3+2} = n_{5,5} = \left|E_{5,5}\right| = 3-1 = 2$.

Now,

$$\begin{aligned} Zg_4(CT(s)\Theta P_n) &= (3+n)(2s+3) + (6+3n)\sum_{i=2}^{s} 2^{i-2}(2(s+i)+1) \\ &+n(12s+9)\left(2^{s-1}\right) + 3(n-1)\sum_{i=1}^{s} 2^{i-1}\times 2(s+i+2) \\ &+6\left(2^{s-1}\right)(2s+1) + 2(n-1)(s+2) \\ &= n(9\times 2^s - 2 + 24s\times 2^s) + s(6\times 2^s - 8n - 2) - 6\times 2^s + 5; \end{aligned}$$

and

$$\begin{aligned} Zg_6(CT(s)\Theta P_n) &= \left(s^2+3s\right)(3+n) + 2(n+3) + (6+3n)\sum_{i=2}^{s} 2^{i-2}(s+i)(s+i+1) \\ &+6n\left(2^{s-1}\right)\left(2s^2+3s+1\right) + 3(n-1)\sum_{i=1}^{s} 2^{i-1}(s+i+2)^2 \\ &+3\left(2^{s-1}\right)(2s+1)^2 + (n-1)(s+2)^2 \\ &= s^2(6\times 2^s - 4n + 24n\times 2^s - 1) + s(5 - 2n - 12\times 2^s + 18n\times 2^s) \\ &\qquad +2^s\left(15n - \tfrac{3}{2}\right) - 9n - 1. \end{aligned}$$

□

All the results follow from the edge partitions defined above and the definitions of the respective indices.

Theorem 8. *The first and second Zagreb, and the atom bond connectivity indices of $CT(s)\Theta P_n$ are given by:*

(i) $M_1(CT(s)\Theta P_n) = (3\times 2^s - 2)\left(n^2 + 15n - 1\right)$;

(ii) $M_2(CT(s)\Theta P_n) = ((3\times 2^s - 2)\left(9n^2 + 50n - 15\right))/2$;

(iii) $ABC(CT(s)\Theta P_n) = \frac{(9\times 2^s - 6)}{2}\times\frac{\sqrt{2(n+2)}}{(n+3)} + 2(3\times 2^s - 2)\sqrt{\frac{1}{2}} + (n-2)(3\times 2^s - 2)\sqrt{\frac{(n+4)}{(3)(n+3)}} + (3\times 2^s - 2)\sqrt{2} + (n-3)(3\times 2^s - 2)(2/3)$.

Proof. Let the vertex and edge partitions of $CT(s)\Theta P_n$ be given by:

- $P_1 = \left\{v\middle|\, d(v) = 2\right\}$ and $|P_1| = 2(3\times 2^s - 2)$;
- $P_2 = \left\{v\middle|\, d(v) = 3\right\}$ and $|P_2| = (n-2)(3\times 2^s - 2)$;
- $P_3 = \left\{v\middle|\, d(v) = n+3\right\}$ and $|P_3| = (3\times 2^s - 2)$:

and

- $E_{n+3,n+3} = \{e = uv \in E(CT(s)\Theta P_n)\,\big|d(u) = n+3 \text{ and } d(v) = n+3\}$ and $\left|E_{n+3,n+3}\right| = (9\times 2^s - 6)/2$;
- $E_{2,n+3} = \{e = uv \in E(CT(s)\Theta P_n)\,\big|d(u) = 2 \text{ and } d(v) = n+3\}$ and $\left|E_{2,n+3}\right| = 2(3\times 2^s - 2)$;
- $E_{3,n+3} = \{e = uv \in E(CT(s)\Theta P_n)\,\big|d(u) = 3 \text{ and } d(v) = n+3\}$ and $\left|E_{3,n+3}\right| = (n-2)(3\times 2^s - 2)$;
- $E_{2,3} = \{e = uv \in E(CT(s)\Theta P_n)\,\big|d(u) = 2 \text{ and } d(v) = 3\}$ and $\left|E_{2,3}\right| = 2(3\times 2^s - 2)$;
- $E_{3,3} = \{e = uv \in E(CT(s)\Theta P_n)\,\big|d(u) = d(v) = 3\}$ and $\left|E_{3,3}\right| = (n-3)(3\times 2^s - 2)$.

Now,

$$M_1(CT(s)\Theta P_n) = \sum_{v\epsilon P_1}(d(v))^2 + \sum_{v\epsilon P_2}(d(v))^2 + \sum_{v\epsilon P_3}(d(v))^2$$
$$= 2(3\times 2^s-2)\left(2^2\right) + (n-2)(3\times 2^s-2)\left(3^2\right) + (3\times 2^s-2)(n+3)^2$$
$$= (3\times 2^s-2)\left(n^2+15n-1\right);$$

$$M_2(CT(s)\Theta P_n) = \tfrac{(9\times 2^s-6)}{2}(n+3)^2 + 2(3\times 2^s-2) + ((2)(n+3))$$
$$+(n-2)(3\times 2^s-2)((3)(n+3)) + 2(3\times 2^s-2)((2)(3))$$
$$+(n-3)(3\times 2^s-2)((3)(3))$$
$$= ((3\times 2^s-2)\left(9n^2+50n-15\right))/2;$$

Likewise, we can obtain $ABC(CT(s)\Theta P_n)$. □

Remark 5. *The results obtained from Topo-Chemie-2020 [40] are shown in Table 4 for a comparison with the results obtained from Theorems 7 and 8.*

Table 4. Results obtained for the corona product $CT(s)\Theta P_n$ of a Christmas tree $CT(s)$ and a path P_n with the computer code, compared with the results from the expressions in Theorems 7 and 8.

Index	Dimension s, n	From Expressions 7 and 8	Topo-Chemie-2020 [40]
$GA_4(CT(s)\Theta P_n)$	$s=3, n=3$	142.7317	142.73175770071703
	$s=4, n=4$	390.5798	390.5798602154981
$Zg_4(CT(s)\Theta P_n)$	$s=3, n=3$	1961	1961
	$s=4, n=4$	6869	6869
$\Pi_4^*(CT(s)\Theta P_n)$	$s=3, n=3$	$9.65986697\times 10^{161}$	$9.659866968127555\times 10^{161}$
	$s=4, n=4$	Infinity	+Inf
$Zg_6(CT(s)\Theta P_n)$	$s=3, n=3$	6824	6824
	$s=4, n=4$	30,567	30,567
$\Pi_6^*(CT(s)\Theta P_n)$	$s=3, n=3$	4.3849717×10^{237}	$4.384971723725398\times 10^{237}$
	$s=4, n=4$	Infinity	+Inf
$ABC_5\Pi(CT(s)\Theta P_n)$	$s=3, n=3$	$1.4118921672\times 10^{-43}$	$1.411892167070263\times 10^{-43}$
	$s=4, n=4$	$6.08702627\times 10^{-136}$	$6.087026262790365\times 10^{-136}$
$M_1(CT(s)\Theta Pn)$	$s=3, n=3$	1166	1166
	$s=4, n=4$	3450	3450
$M_2(CT(s)\Theta Pn)$	$s=3, n=3$	2376	2376
	$s=4, n=4$	7567	7567
$ABC(CT(s)\Theta Pn)$	$s=3, n=3$	93.33733429352	93.33733429351358
	$s=4, n=4$	251.70409168311	251.70409168311375

4. Various Applications of Topological Indices for the COVID-19 Pandemic

There are two types of emerging applications of graph theory and topological indices. One of the more well studied applications of topological indices is the prediction of physicochemical properties and biological activities of chemicals and drugs through an approach called the quantitative structure activity relation (QSAR). This approach relies on the fact that the property of a molecule bears a mathematical relation to the structure or the associated connectivity of the molecule. In this context, several topological indices have been shown to statistically correlate with a number of observable properties such as dermal penetration, protonation constants, chromatographic retention indices,

lipophilicity, octanol partition coefficients, and so on [11,45,46]. When topological indices are combined with other quantum chemically derived electronic parameters [46–49] such as the Highest Occupied Molecular Orbital (HOMO)- Lowest Unoccupied Molecular Orbital (LUMO) energy gaps, hardness, softness, polarizability, molecular electrostatic potentials, Natural Bond Orbital (NBO) analysis, etc., one could obtain quantitative measures of the relative stabilities, reactivities and binding potentials of a drug as a viral inhibitor which can then assist in finding potential cures for the severe acute respiratory syndrome coronavirus 2 (SARS-CoV-2). One could invoke statistical techniques such as the principal component analysis by including several of the indices developed in this study to discover among various topological indices which ones would offer the best correlation and predictive power compared to the observed properties [46–49].

For example, it has been shown earlier [45] that the log$P$ values of polyacenes have a very good correlation with the Szeged index that we computed in the present study using Theorem 1, as per the following statistical correlation:

$$\log P(Lh) = 1.0875 \times 10^{-4} Sz + 9.210,$$

with an r value of 0.9258. We anticipate a similar correlation for the potential drugs for the coronavirus-2, although the actual additive and multiplier constants would depend on available experimental data for these compounds.

In a recent work, Mondal et al. [47] studied degree-based and neighborhood degree sum-based topological indices in order to provide structure-activity correlations for a set of investigated antiviral drugs for COVID-19 such as remdesivir (GS-5734), chloroquine, hydroxychloroquine, theaflavin, etc., by using graph polynomial approaches. Mondal et al. [47] noted that the results obtained from such topological studies can aid in the development of potentially new drugs for the treatment of COVID-19, although it is skeptical that topological indices alone can result in the discovery of new drugs. It can, however, be stated that the developed indices have the efficacy to predict many properties and activities such as boiling point, entropy, enthalpy, acentric factor, vapor pressure etc., as these properties do not depend on guest–host interactions and exhibit direct structural dependency. However, the discovery of potentially new drugs needs more sophisticated approaches such as quantum chemical docking, molecular dynamics etc., [48–50] that focus on the viral protease–drug inhibitor interactions in order to enhance the efficacy of a drug as an inhibitor of severe acute respiratory syndrome coronavirus 2 (SARS-CoV-2) protease. Consequently, in the area of drug discovery, topological indices play a limited role, that is, only as starting points for molecular similarity and QSAR analysis, and in the selection of various ligands from a library. Moreover, topological indices cannot serve as the end point in silico drug discovery for which sophisticated tools based on quantum mechanics are required to analyze and understand the guest–host interactions involved in potential drug discovery [48–50]. Figures 6 and 7 show the 3D plots of log of the Szeged and fourth geometric-arithmetic indices respectively for pandemic trees. As can be seen from Figure 6, the magnitude of log of Szeged index for $k = 6$ at a given level is several orders larger than that of $k = 2$ at the same level. This clearly demonstrates the severity of the ongoing COVID-19 which has a R^0 value close to 6 in a susceptible population set compared to $k = 2$ for the 1918 Spanish flu. As seen from Figure 7, we obtain a similar trend for the log of the fourth geometric-arithmetic indices for pandemic trees.

Plots such as the ones obtained in these figures from the computed topological indices provide significant new insights into the severity of the ongoing COVID-19 pandemic, underscoring the importance of intervention steps not only through quarantining but also through several other mitigation measures such as therapeutic interventions, vaccines and improved public awareness of hygiene, social distancing, facial shields, masks, and other measures to prevent the spread.

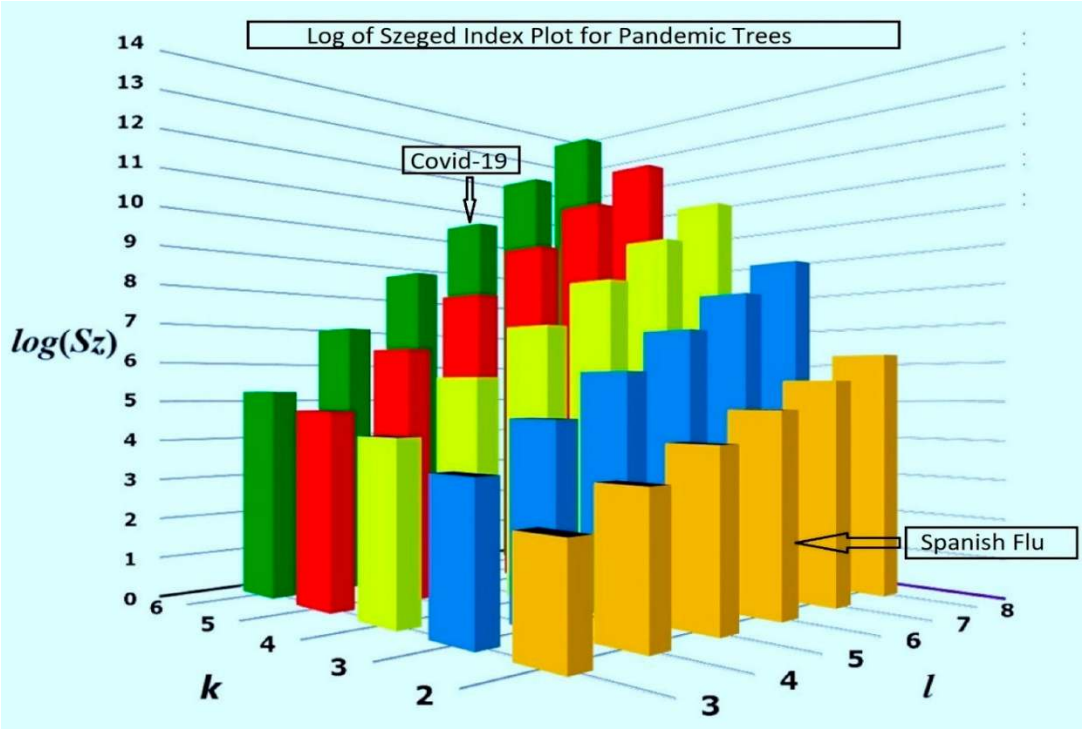

Figure 6. log(Sz) values obtained for the Szeged index of pandemic trees T_l^k demonstrate the underlying severity of COVID-19 as compared to the 1918 Spanish flu.

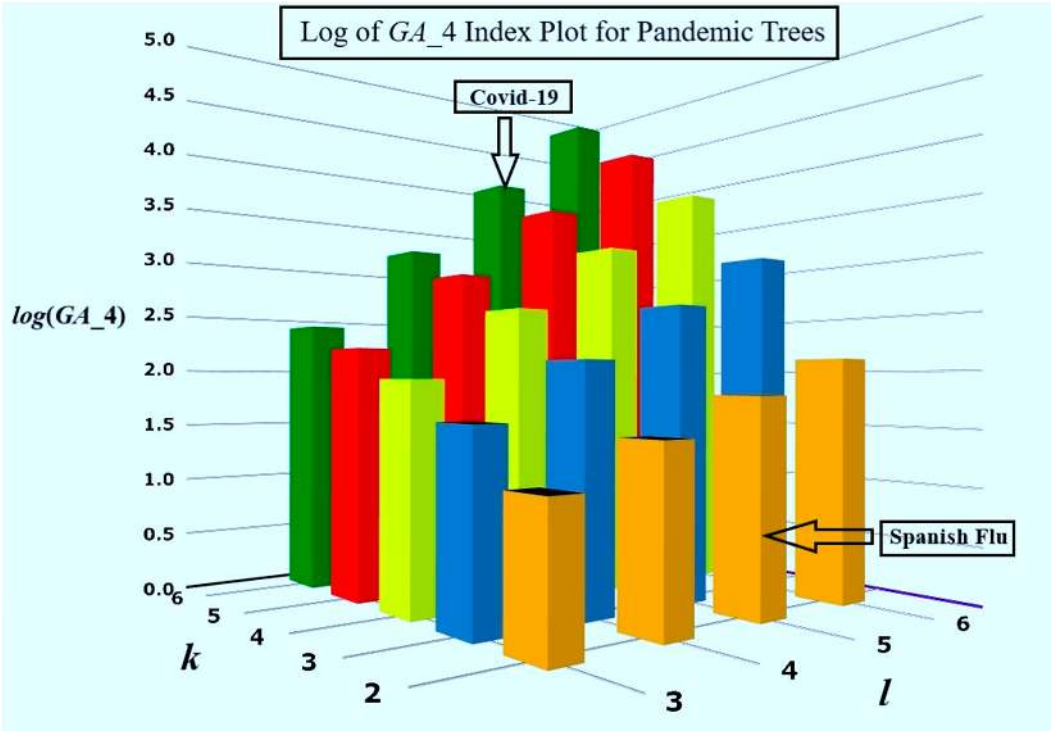

Figure 7. log(GA_4) values obtained for the fourth geometric-arithmetic index of pandemic trees T_l^k demonstrate the underlying severity of COVID-19 as compared to the 1918 Spanish flu.

The second area where our developed topological indices may help us in understanding of the evolutionary dynamics of the COVID-19 pandemic in terms of genomics is in the identification of various mutations of the genes that occur during the epidemic propagation, and in the evolutionary

relationship of the mutations as a function of the propagation to the presumed genome of the Wuhan bat origin. Secondly, the graph theoretical network aids in enhancing our understanding of the dynamics of the spread of the pandemic as a function of regions, sectors, states or provinces, and countries.

In relationship to the epidemiological dynamics, as several of the topological indices that we computed here are eccentricity-based indices, they measure the extent of the spread and the magnitude of the effect of the pandemic (see Figures 6–8) on a given population set. Another important feature of the topological indices considered here is that the indices can provide insight into the effect of the introduction of an infected individual in a pool of uninfected individuals through vertex coloring to identify the infected person and recomputing the indices with the resulting weighted graphs. As the topological indices computed here vary as a function of level, one obtains quantitative measures in terms of these indices of the epidemic progression at different levels. Graph theoretical tools developed here can facilitate juxtaposing different scenarios by superposing one network over the other, for example, under the conditions that a given individual infects 2 others compared to an individual infecting 4 other individuals and so on. Consequently, the network analysis presented here can aid in the development of artificial intelligence tools in a computer-assisted study of the epidemiological dynamics of the pandemic, and thus in the development of mitigation strategies. There are several such applications of these indices which can become the topic of future studies.

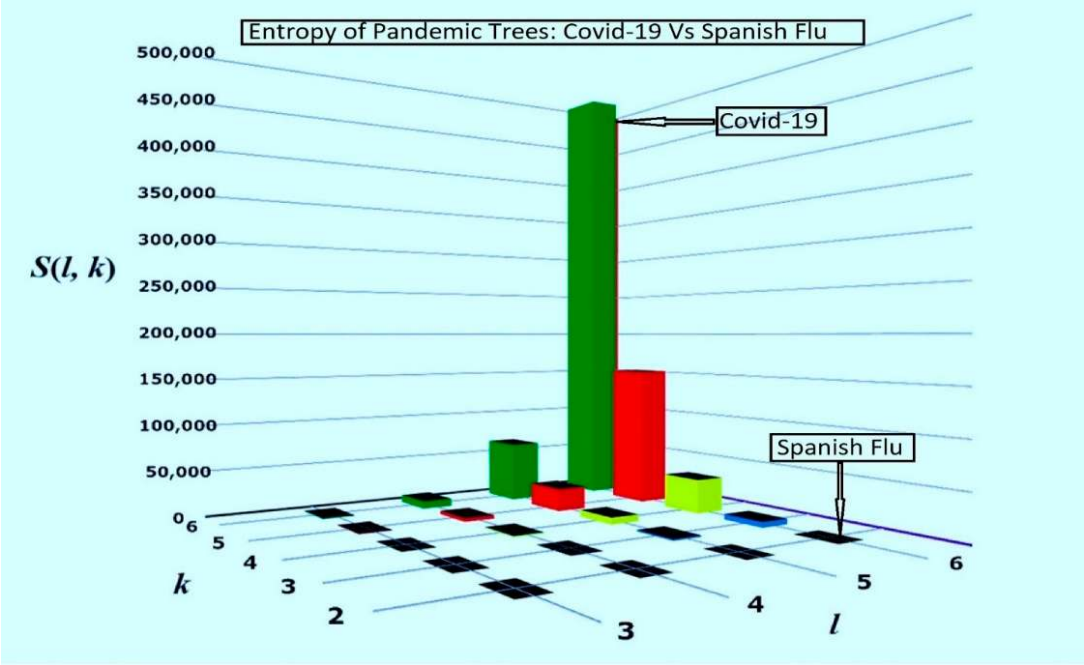

Figure 8. Entropy values measured in the units of k_B or $S(l, k)$ obtained for pandemic tree T_l^k accentuates the underlying severity of COVID-19 compared to the 1918 Spanish flu.

It should be emphasized that all of the topological indices in Section 4 and entropies obtained in Section 5 and comparisons that are made, are based on the assumed R^0, which is a result of the illness itself and various interventions. It is a macroscopic rather than a microscopic measure. Thus, the comparison made here is by no means indicative of the total number of infections or deaths, as they depend on multiple factors such as the discovery of vaccines, adherence to social distancing, more advanced technological tools available today for diagnosis, contract tracing, treatments, mitigation measures, and prognosis compared to 1918. Hence, there are several substantial differences between the two pandemics, namely COVID 19 and the Spanish Flu. First, they are both caused by different types of viruses with different modes of infection. We have denser populations and a far more connected world with air travel which can contribute to the spread of COVID-19 globally. Specifically, the comparisons of Covid-19 and Spanish flu provided in this section do not take directly into consideration a number

of factors enumerated below which could alter the assumed R^0 values dynamically and hence the computed indices:

1. The difference in the awareness among all the countries and the general population on the severity of the disease and the necessary preventive actions that are needed as a result of internet and other forms of communications.
2. The difference in the resources available for healthcare.
3. The difference in number of qualified and trained virologists, doctors, nurses, government officials, government/private institutions, and other important frontline workers.
4. The difference in information content available through research, innovations, and the data from the past pandemic, all of which can contribute to improved predictions. Researchers worldwide are working diligently to find a vaccine against the virus causing the COVID-19 pandemic. The WHO is working in collaboration with scientists, business, and global health organizations to accelerate the vaccine effectiveness and discovery [51].
5. Other social, economic, and medical changes that occurred in the last 100 years.

Therefore, comparisons of entropies computed in Section 5 and other topological indices in this section were made with presently available R^0 for COVID-19, which itself could dynamically change with discoveries of vaccine, technological advances to effectively control the epidemic and the role of super spreaders. Furthermore, entropy measures from Section 5 suggest that the ongoing pandemic left to itself without such mitigating measures, poses an enormous and unique challenge globally, and the ongoing battle is nowhere near the end. Hence, significant interventions and countermeasures must be taken such as therapeutic interventions including vaccines, social distancing, vigorous quarantine measures, facial masks, improved oral and hand hygiene measures. The availability of preventive and therapeutic tools against viral infections and their related complications is an important factor for the disaster risk assessment [52].

5. Thermodynamic Entropy of Pandemic Trees

As demonstrated earlier, a complete k-ary tree T_l^k is the pandemic tree with an R^0 value of k. The R^0 epidemiological measure is exponential similar to other natural disasters such as an earthquake measured in a logarithmic Richter scale. We introduce here yet another measure of the chaos created by the COVID-19 pandemic which is based on the thermodynamic Boltzmann's definition of entropy, a measure of the degree of disorder. At the very outset, it is pointed out that the thermodynamic entropy is different from the graph theoretical entropy discussed by Dehmer and co-workers [53–55] although in principle there should be a correspondence between statistical thermodynamic entropy and information theoretic entropy. The graph theoretical entropy concept invoked by these authors is based on Shannon's information theoretic formulation as applied to graph theoretical invariants. On the other hand, the thermodynamic entropy is simply based on the celebrated Boltzmann's definition and formula for the entropy. Consequently, in the present study, the term entropy refers to the thermodynamic entropy which is simply based on the number of distinct configurations or the number of inequivalent ways to label the vertices of a graph under the action of the automorphism group of the graph. The set R^{D} of functions from the set D of vertices to the set R of colors would form equivalence classes under the action of the automorphism group. Among these classes, the number of classes where each vertex is colored with a unique color corresponds to the number of unique ways to label the graph, and hence, this number measures the number of distinct configurations a graph can take under the group action.

The entropy of a pandemic tree is measured directly by the number of unique ways of labeling the pandemic tree. In general, the number of inequivalent ways to label any graph with n vertices is given by:

$$N_{Lab} = \frac{n!}{\left|Aut(G)\right|},$$

where $Aut(G)$ is the automorphism group of the graph G under consideration, and $|Aut(G)|$ is the number of elements in the automorphism group. The automorphism group of a graph with n vertices is defined as edge-preserving permutations of the vertices or it is comprised of those permutations of the vertices with permutation matrices P satisfying the condition:

$$A = P^T AP,$$

where A is the adjacency matrix of the graph. The automorphism groups of several types of polyhedral graphs were studied recently by Ghorbani et al. [56].

Balasubramanian [15] previously studied the automorphisms of Cayley trees, complete k-ary trees, etc., and showed that the automorphism group of a T_l^k tree with l levels is given by:

$$Aut\left(T_l^k\right) = S_k[S_k[S_k \ldots\ldots] \ldots\ldots],$$

where the group is a nested wreath product of the symmetric group S_k recurring l times in the above product. The wreath product [15] of two groups G and H denoted by $G[H]$ is a group defined by $(H_1\ x\ H_2\ x \ldots\ H_n)\hat{}\ G'$, where x is a direct product of two groups, $\hat{}$ is a semi-direct product and G' is a group isomorphic with G acting on the whole set of vertices. The group is comprised of $|H|^n|G|$ operations. The order of each S_k group composing the wreath product of a pandemic tree is $k!$. The order of a nested wreath product group was obtained by Balasubramanian [15] as:

$$|\{[S_k]\}^l| \ = \ (k!)^{a_l}, \ a_l = \frac{\left(k^l - 1\right)}{(k-1)}.$$

As it was shown in a previous section, the number of vertices in $T_l^k = a_{l+1} = \frac{k^{l+1}-1}{k-1}$, we arrive at the result for the number of unique ways to label a pandemic tree T_l^k as:

$$N_{Lab} \ = \ \frac{(a_{l+1})!}{(k!)^{a_l}},$$

where N_{Lab} is also referred to as the number of different configurations denoted by Ω in statistical mechanics. The entropy of any system, denoted by S, is defined by the Boltzmann equation and it measures the degree of disorder. It is given by:

$$S = k_B \ln(\Omega),$$

where k_B is the Boltzmann constant.

We can obtain the entropy $S(l, k)$ of a pandemic tree using the above equation with Ω defined as the number of inequivalent ways of labeling the pandemic tree that we have obtained above. This combined with the Stirling approximation for the factorial of any large number, we arrive at the following expression for $S(l, k)$ of a pandemic tree T_l^k as:

$$S(l,k) = k_B\{a_{l+1}\ln(a_{l+1}) - a_{l+1} + \tfrac{1}{2}\ln(2\pi a_{l+1}) - a_l \ln(k!)\},$$
$$a_{l+1} = \tfrac{k^{l+1}-1}{k-1}.$$

In Figure 8 we have plotted $S(l, k)/k_B$ as function of both k and l, and we can see that the order of S increases as a function of k and l. This shows the severity of the ongoing pandemic which has a k value of 6 and as l goes to 6 nearly the entire susceptible population is infected. Moreover, the entropy measure of the ongoing COVID-19 pandemic is dramatically larger than that of the 1918 Spanish flu virus, underscoring the severity on the novel coronavirus 2. Furthermore, entropy is measured in natural logarithmic scale analogous to the Richter scale of an earthquake and thus the ratios of the

entropies of COVID-19 to Spanish flu of 1104.6 at level 6 would suggest about 10^3 greater severity as measured in a natural log scale. Thus, entropy provides yet another quantitative measure for the epidemiologists to measure the degree of disorder and hence the severity of the ongoing pandemic.

6. Stochasticity in Pandemic Tree Generation

Our study so far has captured the worst case, when an infected individual spreads the infection to R^0 other individuals, by studying a complete k-ary tree with $k = R^0$ as a particular case. This may not be the case always except in worst affected locations. In such cases, the pandemic trees will just be R^0-ary trees. Stochasticity in the generation of such trees leads to considering the adjacency matrices of the trees for implementing distance-based graph algorithms. Degree and eccentricity-based topological indices can be easily computed from these matrices.

As an illustration, a random tree T of level $l = 6$ with epicenter of degree $R^0 = 6$ at level 0 and with every vertex of level i having R^0-i children, $0 \leq i \leq 5$, is considered in Figure 9.

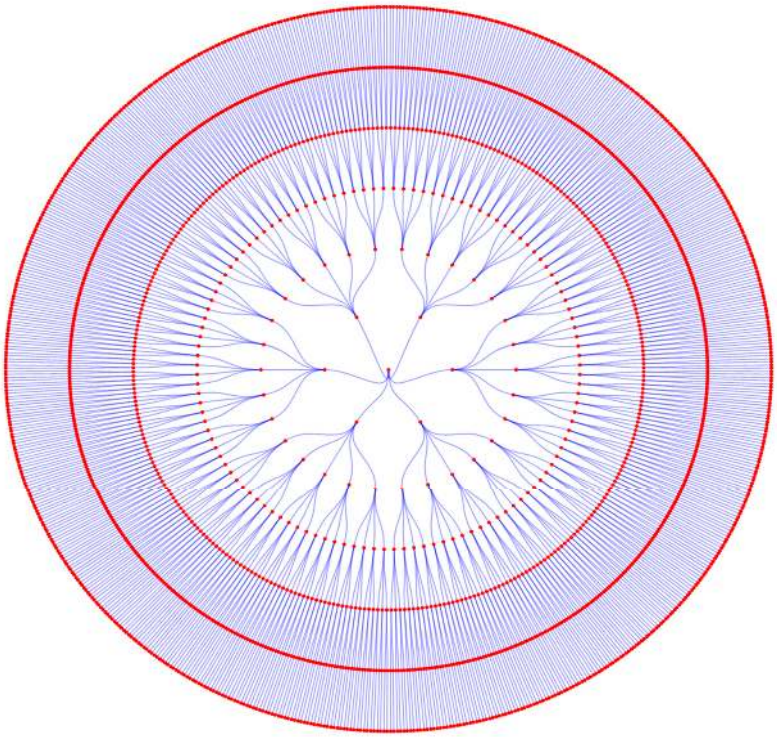

Figure 9. A random tree T with epicenter of degree 6.

A few topological indices of this tree T of level $l = 6$ are listed below:

1. $M_1(T) = \sum_{v_i \in V(T)} d_i^2 = 1957l^2 - 15{,}660l + 33{,}270$;
2. $M_2(T) = \sum_{v_i v_j \in E(T)} d_i d_j = 1956l^2 - 13{,}710l + 25{,}440$;
3. $ABC(T) = \sum_{v_i v_j \in E(T)} \sqrt{\frac{d_i + d_j - 2}{d_i d_j}} = \left(\frac{\sqrt{10}}{6}\right)l + 30\sqrt{\frac{2l-3}{l^2-l}} + 120\sqrt{\frac{2l-5}{l^2-3l+2}} + 360\sqrt{\frac{2l-7}{l^2-5l+6}} + 120\sqrt{\frac{2l-9}{l^2-7l+12}} + 720\sqrt{\frac{2l-11}{l^2-9l+20}}$;
4. $PI(T) = \sum_{e=uv \in E(T)} [n_u(e) + n_v(e)] = 1957l + 3{,}816{,}150$;
5. $Sz(T) = \sum_{e=uv \in E(T)} [n_u(e) \times n_v(e)] = 531{,}706l + 15{,}153{,}306$.

Evidently such generation of random k-ary trees needs to be considered through computational techniques based on algorithms such as the Monte Carlo algorithm and subsequent iterative computation of the various topological indices numerically. Such a technique would also encompass the possibility of including a super spreader in the random pandemic tree.

7. Conclusions

In the current study, we have shown that the developed topological indices play an important role in quantifying the network information contained in pandemic trees. Furthermore, the graph theoretical techniques presented here can aid in a number of predictions concerning the dynamics of the ongoing pandemic, for example, how the introduction of an infected person in a pool of uninfected group would alter the spread dynamics. This is tantamount to introducing a new vertex in the tree and associated edges. Then, one can recompute the various topological indices to see how the pandemic evolves as a function of perturbations and quarantines. Such detailed investigations specific to the pandemic can be the topic of future studies. Finally, we computed the entropies of pandemic trees and the related Cayley trees, which provided significant new insights into the severity of the ongoing COVID-19 pandemic as compared to the 1918 Spanish flu which pales into insignificance in terms of entropy and topological measures compared to the severity of COVID-19.

Author Contributions: Conceptualization, K.B., R.S.R. and G.K.N.; methodology, K.B., R.S.R., G.K.N. and A.A.S.; software, K.B.; validation, K.B., T.M.R., G.K.N. and A.A.S.; formal analysis, K.B., I.R.; investigation, R.S.R. and G.K.N.; resources, K.B.; data curation, K.B.; writing—original draft preparation, R.S.R., G.K.N., A.A.S., T.M.R. and I.R.; writing—review and editing, K.B. and R.S.R.; visualization, K.B. and R.S.R.; supervision, R.S.R., K.B. and I.R.; project administration, R.S.R.; funding acquisition, R.S.R. All authors have read and agreed to the published version of the manuscript.

Funding: The work of R. Sundara Rajan is supported by Project No. ECR/2016/1993, Science and Engineering Research Board (SERB), Department of Science and Technology (DST), Government of India.

Acknowledgments: The authors sincerely thank the reviewers for their comments and suggestions which significantly improved the quality of this paper. Further, we thank A. John Sujith, Alagappa University, Karaikudi, and K. Jagadeesh Kumar, Department of Mathematics, Hindustan Institute of Technology and Science, Chennai, India, for their fruitful suggestions.

Conflicts of Interest: The authors declare that there is no conflict of interest regarding the publication of this paper.

References

1. Whitelaw, S.; A Mamas, M.; Topol, E.; Van Spall, H.G. Applications of digital technology in COVID-19 pandemic planning and response. *Lancet Digit. Health* **2020**, *2*, e435–e440. [CrossRef]
2. Blackwood, J.C.; Childs, L.M. An introduction to compartmental modeling for the budding infectious disease modeler. *Lett. Biomath.* **2018**, *5*, 195–221. [CrossRef]
3. Zhou, P.; Yang, X.-L.; Wang, X.-G.; Hu, B.; Zhang, L.; Zhang, W.; Si, H.-R.; Zhu, Y.; Li, B.; Huang, C.-L.; et al. A pneumonia outbreak associated with a new coronavirus of probable bat origin. *Nature* **2020**, *579*, 270–273. [CrossRef]
4. Lai, C.-C.; Shih, T.-P.; Ko, W.-C.; Tang, H.-J.; Hsueh, P.-R. Severe acute respiratory syndrome coronavirus 2 (SARS-CoV-2) and coronavirus disease-2019 (COVID-19): The epidemic and the challenges. *Int. J. Antimicrob. Agents* **2020**, *55*, 105924. [CrossRef]
5. Andersen, K.G.; Rambaut, A.; Lipkin, W.I.; Holmes, E.C.; Garry, R.F. The proximal origin of SARS-CoV-2. *Nat. Med.* **2020**, *26*, 450–452. [CrossRef]
6. Zhou, F.; Yu, T.; Du, R.; Fan, G.; Liu, Y.; Liu, Z.; Xiang, J.; Wang, Y.; Song, B.; Gu, X.; et al. Clinical course and risk factors for mortality of adult inpatients with COVID-19 in Wuhan, China: A retrospective cohort study. *Lancet* **2020**, *395*, 1054–1062. [CrossRef]
7. Cui, J.; Li, F.; Shi, Z.-L. Origin and evolution of pathogenic coronaviruses. *Nat. Rev. Genet.* **2019**, *17*, 181–192. [CrossRef]
8. Wu, J.T.; Leung, K.; Leung, G.M. Nowcasting and forecasting the potential domestic and international spread of the 2019-nCoV outbreak originating in Wuhan, China: A modelling study. *Lancet* **2020**, *395*, 689–697. [CrossRef]
9. Forster, P.; Forster, L.; Renfrew, C.; Forster, M. Phylogenetic network analysis of SARS-CoV-2 genomes. *Proc. Natl. Acad. Sci. USA* **2020**, *117*, 9241–9243. [CrossRef]
10. Balasubramanian, K.; Khokhani, K.; Basak, S.C. Complex Graph Matrix Representations and Characterizations of Proteomic Maps and Chemically Induced Changes to Proteomes. *J. Proteome Res.* **2006**, *5*, 1133–1142. [CrossRef]

11. Basak, S.C.; Grunwald, G.D.; Gute, B.D.; Balasubramanian, K.; Opitz, D. Use of statistical and neural net approaches in predicting toxicity of chemicals. *J. Chem. Inf. Comput. Sci.* **2000**, *40*, 885–890. [CrossRef]
12. Matsen, F.A. Phylogenetics and the Human Microbiome. *Syst. Biol.* **2015**, *64*, e26–e41. [CrossRef]
13. Delucchi, E. Nested set complexes of Dowling lattices and complexes of Dowling trees. *J. Algebraic Comb.* **2007**, *26*, 477–494. [CrossRef]
14. Balasubramanian, K. Tree pruning and lattice statistics on Bethe lattices. *J. Math. Chem.* **1988**, *2*, 69–82. [CrossRef]
15. Balasubramanian, K. Nested wreath groups and their applications to phylogeny in biology and Cayley trees in chemistry and physics. *J. Math. Chem.* **2017**, *55*, 195–222. [CrossRef]
16. Balasubramanian, K. Spectra of chemical trees. *Int. J. Quantum Chem.* **1982**, *21*, 581–590. [CrossRef]
17. Balasubramanian, K. Symmetry groups of chemical graphs. *Int. J. Quantum Chem.* **1982**, *21*, 411–418. [CrossRef]
18. Sellers, P.H. On the Theory and Computation of Evolutionary Distances. *SIAM J. Appl. Math.* **1974**, *26*, 787–793. [CrossRef]
19. Sellers, P.H. An algorithm for the distance between two finite sequences. *J. Comb. Theory Ser. A* **1974**, *16*, 253–258. [CrossRef]
20. Fischer, M.; Klaere, S.; Nguyen, M.A.T.; Von Haeseler, A. On the group theoretical background of assigning stepwise mutations onto phylogenies. *Algorithms Mol. Biol.* **2012**, *7*, 36. [CrossRef]
21. Yun, U.; Lee, G.; Kim, C.-H. The Smallest Valid Extension-Based Efficient, Rare Graph Pattern Mining, Considering Length-Decreasing Support Constraints and Symmetry Characteristics of Graphs. *Symmetry* **2016**, *8*, 32. [CrossRef]
22. Xue, L.; Jing, S.; Miller, J.C.; Sun, W.; Li, H.; Estrada-Franco, J.G.; Hyman, J.M.; Zhu, H. A data-driven network model for the emerging COVID-19 epidemics in Wuhan, Toronto and Italy. *Math. Biosci.* **2020**, *326*, 108391. [CrossRef]
23. Basavanagoud, B.; Desai, V.R.; Patil, S. (β,α)−Connectivity Index of Graphs. *Appl. Math. Nonlinear Sci.* **2017**, *2*, 21–30. [CrossRef]
24. Gao, W.; Wang, W. The Vertex Version of Weighted Wiener Number for Bicyclic Molecular Structures. *Comput. Math. Methods Med.* **2015**, *2015*, 1–10. [CrossRef]
25. Gao, W.; Farahani, M.R.; Shi, L. The forgotten topological index of some drug structures. *Acta. Medica. Mediterr.* **2016**, *32*, 579–585.
26. Gao, W.; Wang, W.; Farahani, M.R. Topological Indices Study of Molecular Structure in Anticancer Drugs. *J. Chem.* **2016**, *2016*, 1–8. [CrossRef]
27. Martínez-Pérez, Á.; Rodriguez, J.M. New Bounds for Topological Indices on Trees through Generalized Methods. *Symmetry* **2020**, *12*, 1097. [CrossRef]
28. Atanasov, R.; Furtula, B.; Škrekovski, R. Trees with Minimum Weighted Szeged Index Are of a Large Diameter. *Symmetry* **2020**, *12*, 793. [CrossRef]
29. Knor, M.; Imran, M.; Jamil, M.K.; Škrekovski, R. Remarks on Distance Based Topological Indices for ℓ-Apex Trees. *Symmetry* **2020**, *12*, 802. [CrossRef]
30. Liu, J.-B.; Shaker, H.; Nadeem, I.; Farahani, M.R. Eccentric Connectivity Index of t-Polyacenic Nanotubes. *Adv. Mater. Sci. Eng.* **2019**, *2019*, 1–9. [CrossRef]
31. Ghorbani, M.; Dehmer, M.; Emmert-Streib, F. Properties of Entropy-Based Topological Measures of Fullerenes. *Mathematics* **2020**, *8*, 740. [CrossRef]
32. Ghorbani, M.; Khaki, A. A note on the fourth version of geometric-arithmetic index. *Optoelectron. Adv. Mat.* **2010**, *4*, 2212–2215.
33. Gao, W.; Wu, H.; Siddiqui, M.K.; Baig, A.Q. Study of biological networks using graph theory. *Saudi J. Biol. Sci.* **2018**, *25*, 1212–1219. [CrossRef]
34. Farahani, M.R.; Kanna, R.M.R. Fourth zagreb index of circumcoronene series of benzenoid. *Leonardo Electron. J. Pract. Technol.* **2015**, *27*, 155–161.
35. Gutman, I.; Trinajstić, N. Graph theory and molecular orbitals. Total φ-electron energy of alternant hydrocarbons. *Chem. Phys. Lett.* **1972**, *17*, 535–538. [CrossRef]
36. Das, K.C.; Gutman, I.; Furtula, B. On atom-bond connectivity index. *Chem. Phys. Lett.* **2011**, *511*, 452–454. [CrossRef]

37. Khadikar, P.V.; Karmarkar, S.; Agrawal, V.K. A Novel PI Index and Its Applications to QSPR/QSAR Studies. *J. Chem. Inf. Comput. Sci.* **2001**, *41*, 934–949. [CrossRef]
38. Gutman, I. A formula for the Wiener number of trees and its extension to graphs containing cycles. *Graph Theory Notes NY* **1994**, *27*, 9–15.
39. Song, C.; Hao, R.-X. Antimagic orientations for the complete k-ary trees. *J. Comb. Optim.* **2019**, *38*, 1077–1085. [CrossRef]
40. Balasubramanian, K. Topo-Chemie-2020 is a package of codes that computes numerous degree-based, distance-based, eccentricity-based, neighbour-based topological indices, characteristic polynomials, matching polynomials, distance polynomials, distance degree vector sequences, walks and self-returning walks, and automorphisms of graphs.
41. Weisstein, E.W. Cayley Tree, MathWorld-A Wolfram Web Resource. Available online: https://mathworld.wolfram.com/CayleyTree.html (accessed on 17 September 2020).
42. Gutman, I.; Dobrynin, A.A. The Szeged index—A success story. *Graph Theory Notes NY* **1998**, *34*, 37–44.
43. Hung, C.-N.; Hsu, L.-H.; Sung, T.-Y. Christmas tree: A versatile 1-fault-tolerant design for token rings. *Inf. Process. Lett.* **1999**, *72*, 55–63. [CrossRef]
44. Nada, S.; Elrokh, A.; Elsakhawi, E.; Sabra, D. The corona between cycles and paths. *J. Egypt. Math. Soc.* **2017**, *25*, 111–118. [CrossRef]
45. Khadikar, P.; Karmarkar, S.; Agrawal, V.; Singh, J.; Khadikar, P.V.; Lukovits, I.; Diudea, M.V. Szeged Index—Applications for Drug Modeling. *Lett. Drug Des. Discov.* **2005**, *2*, 606–624. [CrossRef]
46. Basak, S.C.; Mills, D.; Mumtaz, M.M.; Balasubramanian, K. Use of topological indices in predicting aryl hydrocarbon receptor binding potency of dibenzofurans: A hierarchical QSAR approach. *Indian J. Chem.* **2003**, *42*, 1385–1391.
47. Mondal, S.; De, N.; Pal, A. Topological Indices of Some Chemical Structures Applied for the Treatment of COVID-19 Patients. *Polycycl. Aromat. Compd.* **2020**, 1–15. [CrossRef]
48. Balasubramanian, K.; Gupta, S.P. Quantum Molecular Dynamics, Topological, Group Theoretical and Graph Theoretical Studies of Protein-Protein Interactions. *Curr. Top. Med. Chem.* **2019**, *19*, 426–443. [CrossRef]
49. Balasubramanian, K. Mathematical and Computational Techniques for Drug Discovery: Promises and Developments. *Curr. Top. Med. Chem.* **2019**, *18*, 2774–2799. [CrossRef]
50. Patil, V.M.; Narkhede, R.R.; Masand, N.; Rameshwar, S.; Cheke, R.S.; Balasubramanian, K. Molecular insights into Resveratrol and its analogs as SARS-CoV-2 (COVID-19) protease inhibitors. *Coronaviruses* **2020**, in press.
51. Available online: https://www.who.int/emergencies/diseases/novel-coronavirus-2019/covid-19-vaccines (accessed on 25 November 2020).
52. Javelle, E.; Raoult, D. COVID-19 pandemic more than a century after the Spanish flu. *Lancet Infect. Dis.* **2020**. [CrossRef]
53. Dehmer, M.; Mowshowitz, A. A history of graph entropy measures. *Inf. Sci.* **2011**, *181*, 57–78. [CrossRef]
54. Mowshowitz, A.; Dehmer, M. Entropy and the Complexity of Graphs Revisited. *Entropy* **2012**, *14*, 559–570. [CrossRef]
55. Mowshowitz, A. Entropy and the complexity of graphs: I. An index of the relative complexity of a graph. *Bull. Math. Biol.* **1968**, *30*, 175–204. [CrossRef]
56. Ghorbani, M.; Dehmer, M.; Rahmani, S.; Rajabi-Parsa, M. A Survey on Symmetry Group of Polyhedral Graphs. *Symmetry* **2020**, *12*, 370. [CrossRef]